Oxygen Reduction Reaction Kinetics on Pt in Mixtures of Proton Conducting

Ionic Liquids (PILs) and Water: The Influence of Cation Acidity

K. Wippermann, 1\* Y. Suo<sup>1,2</sup> and C. Korte<sup>1</sup>

<sup>1</sup>Forschungszentrum Jülich GmbH, Institute of Energy and Climate Research – Electrochemical Process

Engineering (IEK-14), 52425 Jülich, Germany

<sup>2</sup>RWTH Aachen University, 52062 Aachen, Germany

\*corresponding author; tel.: +49 2461 61 2572; fax: +49 2461 61 6695; e-mail address:

k.wippermann@fz-juelich.de

**ABSTRACT** 

The aim of this study is to investigate the effect of the acidity of proton conducting ionic liquids (PILs) on

the ORR kinetics at polycrystalline platinum electrodes. Three PILs ([2-SEMA][TfO], [1-EIm][TfO] and

[DEMA][TfO]) with different cation acidities (aqueous p $K_a = 0.94$ , 7.30 and 10.55) are investigated. The

ORR kinetics are evaluated by simulating cyclic voltammograms recorded under an oxygen atmosphere.

An associative mechanism, including H<sub>3</sub>O<sup>+</sup> as the dominant proton donator, is used for the simulations. The

dependencies of the rate constants  $k_1$  and the charge transfer coefficients  $\alpha_1$  of the r.d.s.  $(O_2 + e^- \rightarrow O_2^-)$  on

the cation acidity, the water content ( $\approx 3-50 \text{ mol}\%$ ) and the temperature (30-90 °C), are analyzed. The rate

constant  $k_1$ , the pre-exponential factor of  $k_1$  and the current density are observed to increase with the acidity

of the PIL cation, whereas  $\alpha_1$  shows the opposite behavior. At low water concentrations, the [2-SEMA+]

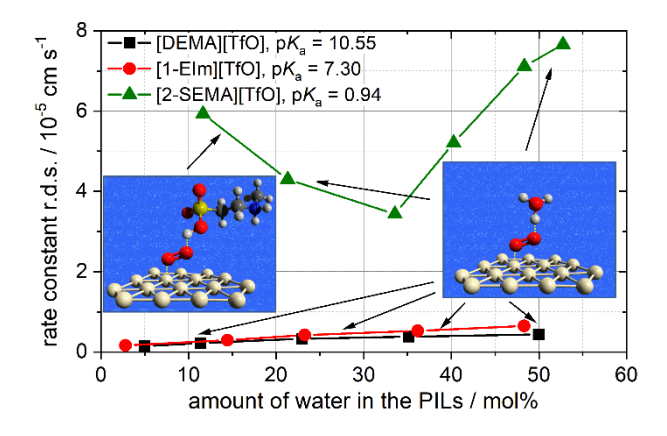
cation is a remarkably good proton donator in ORR, contrary to the former results obtained from the H<sub>UPD</sub>

reaction. This leads to a minimum of  $\approx 30$  mol% in the plots of the current density and  $k_1$  vs. the water

content, which correlates with a similar dependency of the pseudo capacitance  $C_2$ .

1

# TOC Graphic:



Keywords: Acidity; water content; ionic liquids; [2-SEMA][TfO]; [1-EIm]]TfO]; [DEMA][TfO]

# INTRODUCTION

High-temperature polymer electrolyte membrane fuel cells (HT-PEMFCs), operated in a temperature range of 160-180 °C, are based on phosphoric acid ( $H_3PO_4$ )-doped polybenzimidazole (PBI) membranes. The atmospheric operation of low-temperature PEMFCs, using perfluorosulfonic acid (PFSA)-based polymer membranes is restricted to temperatures below 80 °C due to the humidification necessary. Even an operating temperature of 120 °C would be sufficient to simplify water management and allow much more effective cooling and waste heat utilization. However, concentrated phosphoric acid causes a significant decrease in the oxygen reduction reaction (ORR) kinetics on the cathode side because of a poisoning of the Pt catalyst surface by dihydrogen and hydrogen phosphate ions and the low solubility and slow diffusion coefficient of oxygen. A decrease in the operating temperature to 120 °C aggravates the problem, because the ORR kinetics worsens<sup>1</sup> and  $D_{O_2} c_{O_2}$  product decreases further.<sup>2</sup> In fact, no suitable proton-conducting polymer electrolytes are available for this temperature range.

A new approach is the use of proton-conducting (protic) ionic liquids (PIL) as alternative non-aqueous electrolytes in a host polymer such as PBI. A protic ionic liquid must serve as a proton-conducting electrolyte as well as a proton donator in the ORR. In general, ionic liquids have the advantages of a negligible vapor pressure and high chemical and thermal stabilities. Moreover, in the case of proper choice, ionic liquids offer benefits such as a higher  $D_{0_2}c_{0_2}$  product and faster ORR kinetics compared to phosphoric acid. For instance, [DEMA][TfO] (diethyl-methyl-ammonium trifluoromethanesulfonate, see Fig. 1) has a  $D_{0_2}c_{0_2}$  product of  $\approx 5.3 \cdot 10^{-11}$  mol cm<sup>-1</sup> s<sup>-1</sup> (@ 120°C),<sup>3</sup> which is about 30-fold higher than the corresponding value of 98 wt% phosphoric acid ( $\approx 1.9 \cdot 10^{-12}$  mol cm<sup>-1</sup> s<sup>-1</sup>).<sup>2</sup> Several PILs exhibit superior ORR kinetics compared to phosphoric acid, such as [DEMA][TfO],<sup>4</sup> [2-SEA][TfO],<sup>5</sup> (2-sulfoethyl-ammonium trifluoromethanesulfonate) and [2-SEMA][TfO]<sup>6</sup> (2-sulfoethyl-methyl-ammonium trifluoromethanesulfonate; see Fig. 1).

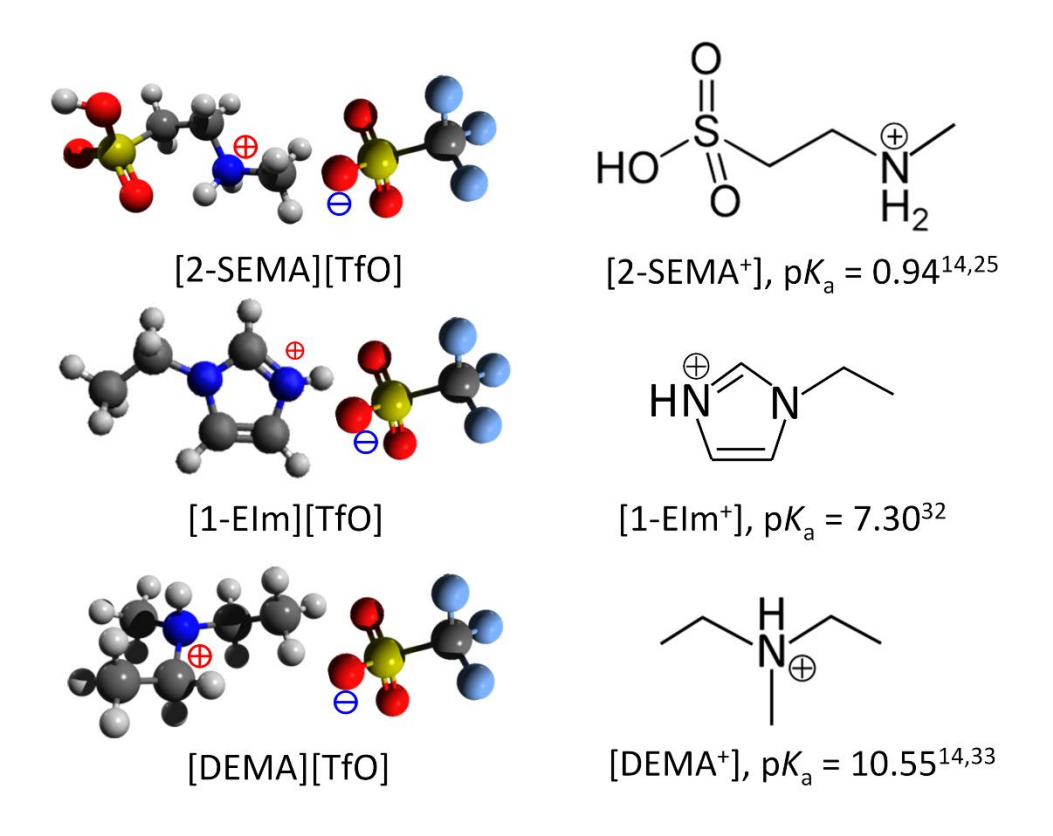


Figure 1. Structures of the PILs and  $pK_a$  values of the cations.

A substantial and systematic improvement in the ORR kinetics requires detailed knowledge about the ORR reaction mechanism(s). The influence of ionic liquid and catalyst properties on the ORR kinetics and mechanisms in energy and sensor systems were recently reviewed by Khan et al.<sup>7</sup> In aprotic, pure ionic liquids (AILs), the generated superoxide anion (O2<sup>•</sup>) can be stable and form part of a reversible ORR process.<sup>8</sup> This can be excluded in neat PILs and binary mixtures of protic ionic liquids and water, where the superoxide anion disproportionates, forming O2<sup>2-</sup>, H2O2, and water.<sup>8-9</sup> In the following, only the latter case will be considered, as under fuel cell operation product water is always generated and protic ionic liquids are required to ensure the necessary ionic charge transport. The ORR kinetics and mechanisms also depend on the nature of the catalyst. The focus herein will be on platinum, which is the state-of-the-art catalyst material for PEMFC electrodes.

In addition to the parameters directly connected to the operating conditions such as temperature and oxygen partial pressure, several properties of protic ionic liquids have been found to influence the ORR kinetics of Pt catalysts, e.g.: (i) the difference in the  $pK_a$  values of Brønsted base (cation precursor) and Brønsted acid (anion precursor),  $\Delta pK_a$ ; (ii) the influence of the adsorption of PIL ions on the surface coverage of oxygen and non-reactive species; (iii) the solubility of oxygen; (iv) the non-stoichiometry of the PIL (e.g., an excess of Brønsted acid); and (v) the molecular structure and properties of the ions, including steric effects, hydrophobicity and the capacity for hydrogen bonding. Most of these properties are closely linked and interdependent.

In aqueous solutions, the change in the free energy  $\Delta G^0$  for the protolysis reaction, *i.e.*, the proton transfer from an acid to a base (e.g., water), is given by:

$$\Delta G^0 = -2.303 RT \Delta p K_a \tag{1}$$

Belieres and Angell<sup>10</sup> used this relationship to calculate the change in the free energy  $\Delta G^0$  for proton transfer during PIL formation based on the  $pK_a$  values of different (organic) bases and acids, forming the cation and anion after protolysis. They noted that these data would enable the thermal stability to be predicted, as well as the ionicity and electrochemical performance of a PIL. Miran et al. <sup>11-12</sup> adopted the approach of Belieres and Angell to characterize the PIL electrolytes utilized in  $H_2/O_2$  fuel cells. Taking the open circuit potential as a measure for the electrocatalytic activity (the higher the catalytic activity, the higher the OCP and the closer its value to the Nernst potential, respectively), they obtained a volcano-like plot of OCP vs.  $\Delta pK_a$ . The maximum OCP at  $\Delta pK_a$  of about 17–18 was explained as follows: if the  $\Delta pK_a$  values and thus the change in the free energy of the proton transfer are too low, the proton transfer from the acid to the base to form the PIL anion and cation is not quantitative and there remain neutral species present. The oxidation of neutral species and the adsorption of the oxidized species on the catalyst causes the ORR performance to deteriorate. <sup>11</sup> In contrast, if the  $\Delta pK_a$  values are too high, more precisely, if the basicity of the cation precursor base is too high and thus the strength of its conjugated acid (PIL cation) is too low the proton activity level in the electrolyte will also be small.

However, it should be noted that the  $pK_a$  values are only valid for diluted solutions. This holds especially true in the case of superacids, for which  $pK_a$  values are experimentally difficult to access and the calculated data varies by orders of magnitude. In this regard, a statement from Trummal et al.<sup>13</sup> is enlightening: "For TfOH, the COSMO-RS value of  $pK_a$  in water was estimated as -4.45, while SMD method provided an aqueous  $pK_a$  range of -12.9 to -18.1." Finally, the acidity of the PILs is not the only factor that determines the ORR kinetics. For these reasons, correlations based on acidity constants yield only semi-quantitative estimates of the optimal  $\Delta pK_a$  values.

Generally speaking, the already mentioned, strong blocking effect of dihydrogen and hydrogen phosphate ions on the Pt cathode catalyst in HT-PEFCs is a key driver in the search for alternative electrolytes with weaker adsorbing anions and cations, such as PILs based on sulfonic acid groups. <sup>5-6, 14-15</sup> Ejigu et al. <sup>16</sup> measured a strongly inhibited ORR in the presence of diethyl-methyl-ammonium bis-(trifluoromethylsulfonyl)-imide [DEMA][Tf<sub>2</sub>N] compared to [DEMA][TfO], with the onset potential of the ORR differing by 900 mV. Besides the explanation of a (too) high  $\Delta pK_a$  value of [DEMA][Tf<sub>2</sub>N], they attributed this highly significant effect to the strong adsorption of [Tf<sub>2</sub>N]<sup>-</sup> ions on the Pt surface, leading to the blocking of active sites. A similar explanation has been offered by Munakata et al., <sup>17</sup> who found that an increasing fluoroalkyl chain length of the imide anions in [DEMA][N(SO<sub>2</sub>(CF<sub>2</sub>)<sub>n</sub>F)<sub>2</sub>] leads to a positive shift in the ORR onset potential, which is caused by decreasing anion adsorption on the Pt surface. Kiatkittikul et al. <sup>18</sup> investigated the influence of the cation structure on the ORR kinetic current on Pt in fluorohydrogenate ionic liquids (FHILs). Amongst various cations, 1-ethyl-1-methylpyrrolidinium [EMPyr]<sup>+</sup> yields the highest ORR activity, which was attributed to the weakest adsorption of [EMPyr]<sup>+</sup> on Pt. These studies reveal that the type of the anion affects the ORR kinetics as well. In particular, [TfO]<sup>-</sup> ions seem to be more suitable for the application of PILs in MT-PEM fuel cells than [Tf<sub>2</sub>N]<sup>-</sup> ions.

Zhang et al.<sup>19</sup> studied the ORR on carbon-supported Pt catalyst impregnated with different amounts of hydrophobic 7-methyl-1,5,7-triazabicyclo[4.4.0]dec-5-en bis-(trifluoromethylsulfonyl)-imide [MTBD][Tf<sub>2</sub>N]. It turned out that the adsorption of PIL ions on the catalyst surface suppresses the formation

of oxygenated species such as OH and Pt oxidation, thus leading to an increased number of free sites for the adsorption of oxygen and enhanced ORR activity. Based on earlier works, *e.g.*, of Snyder et al.,<sup>20</sup> Zhang et al. assumed that higher oxygen solubility in the PIL would significantly contribute to increased ORR activity. Although this assumption was not confirmed in later studies by Zhang et al.<sup>21</sup> and Huang et al.,<sup>22</sup> enhanced oxygen solubility should increase the oxygen surface concentration, the exchange current density of the ORR and so the ORR activity.

As was observed by Kudo et al.,<sup>23</sup> a mixture of 11 mol% trifluoromethanesulfonic acid (TfOH) / 89 mol% [1Et3MeIm][TfO] results in a higher ORR current density compared to pure [1Et3MeIm][TfO]. Clearly, an excess of a strong Brønsted acid accelerates the proton transfer to oxygen and so the overall ORR kinetics. A similar effect was reported by Goodwin et al.:<sup>24</sup> compared to stoichiometric, neat [DEMA][TfO], an excess of 107 mM TfOH in [DEMA][TfO] induces a positive shift in the ORR onset potential by 800 mV. Goodwin et al. explained this strong effect by reference to a change in the proton donor from the very weak acid [DEMA]<sup>+</sup> (p $K_a = 10.55 \pm 0.25^{14,25}$ ) to the superacid TfOH (p $K_a = -14.7 \pm 2.0$ ).<sup>13</sup> These examples demonstrate that the ORR onset potentials of PILs with weakly acidic cations must be interpreted with care, because even a very small excess of a highly acidic anion precursor may cause significant shifts in the onset potential.

Amongst the effects of the structural properties, the influence of the fluoroalkyl chain length of perfluorinated alkanesulfonate anions on the ORR onset potential<sup>17</sup> and the relationship between cation structure and adsorbability<sup>18</sup> has already been mentioned. Stoimenovski et al.<sup>26</sup> found that for the preparation of ammonium-based PILs, an almost full protonation of the amines requires  $\Delta p K_a \ge 4$  in the case of primary amines, but  $\Delta p K_a > 10$  for tertiary ones. This is primarily due to the higher ability of the primary amines to form energetically stabilizing hydrogen bonds. The number of binding sites in PIL cations forming hydrogen bonds was found to correlate with the water uptake/hygroscopicity of PILs.<sup>14</sup> For instance, the (equilibrium) water-to-PIL ratio is 1:1 for [DEMA][TfO] (1 H binding site) and 6:1 for the strongly hygroscopic [2-SEMA][TfO] (5 H binding sites) at RT and a RH  $\approx 49\%$ .<sup>14</sup>

As was noted above, fuel cell operation with PIL electrolytes implies the presence of a few wt% of water. If a superacid like TfOH is used as a precursor for the PIL anion,  $\Delta p K_a$  is high and a reprotonation of the anion can be neglected. Thus, only the protolysis equilibrium of the cation and water must be considered:

$$BH^+ + H_2O \rightleftharpoons B + H_3O^+$$
 (2)

The benefits of a highly acidic cation are manifold: (i) the proton-donating ability of BH+ in ORR is improved; (ii) more H<sub>3</sub>O<sup>+</sup>, which is the dominating ORR proton donator in aqueous acid solutions, is generated according to Eq. (2); (iii) a higher  $H_3O^+$  concentration enables faster proton transport to the Pt surface via the hopping mechanism; (iv) the protonation of a (basic) host membrane and thus the immobilization of the PIL in the membrane is favored. Apart from the above-mentioned influence of the acidity of PILs on the ORR, only a few studies have been published on the influence of water and the PIL cation acidity on the H<sub>UPD</sub> and Pt oxidation/reduction, 14 the effect of water on the double layer properties of metal/PIL or metal/AIL interfaces, 15, 27 the adsorption of water on the Pt in AILs 28-30 and the influence of small amounts of water in AILs on the ORR.<sup>31</sup> In our recent work, we noted a tendency towards increasing the ORR current density with increasing water content in [2-SEMA][TfO].<sup>6</sup> However, to the best of our knowledge, the combined effects of the water content in PILs and the acidity of the PIL cations on the ORR kinetics on Pt have yet to be examined. In this study, the ORR kinetics of the polycrystalline Pt in the presence of PILs with three different cations covering a p $K_a$  range of 0.94–10.55 and a varying water content of about 0.2–7 wt% ( $\approx 3-50$  mol%) are investigated. These PILs are [DEMA][TfO] (p $K_{a \text{ [DEMA]}+} = 10.55^{14}$ , <sup>25</sup>), 1-Ethylimidazoliumtriflate [1-EIm][TfO] ( $pK_{a [1-EIm]+} = 7.3^{32}$ ) and [2-SEMA][TfO] ( $pK_{a [2-SEMA]+} = 0.94^{14}$ ,  $^{33}$ ). Their structural formulas and aqueous p $K_a$  values (valid for diluted aqueous solutions) are shown in

Figure 1. The cyclic voltammograms with these PILs were recorded under an oxygen atmosphere. The simulation of the CVs yielded rate constants and charge transfer coefficients of the r.d.s. dependently of the cation acidity, water content and operating temperature.

## **EXPERIMENTAL**

## PILs and PIL/water mixtures:

[1-EIm][TfO] and [DEMA][TfO] were purchased from IoLiTec-Ionic Liquids Technologies GmbH and used as received without further purification. The nominal purities were > 98 wt% for both [1-EIm][TfO] and [DEMA][TfO]. The water content measured by Karl-Fischer titration (852 Titrando/Metrohm company) was 1300 ppm (0.13 wt%, [1-EIm][TfO]) and 1800 ppm (0.18 wt%, [DEMA][TfO]). [2-SEMA][TfO] was prepared in-house by slowly adding trifluoromethanesulfonic acid (reagent grade, 98%, Sigma Aldrich) to 2-methylaminoethansulfonic acid (N-methyltaurine,  $\geq 99$  %, Sigma Life Science). Karl-Fischer titration yielded a water content of 6400 ppm (0.64 wt%). More details of the preparation process used can be found in Wippermann et al. H NMR spectra of [2-Sema][TfO], [1-EIm][TfO] and [Dema][TfO] have been recently published in Lin et al. By adding appropriate amounts of pure water (Milli-Q®), binary mixtures of water and ionic liquids with up to 7 wt% of water ( $\approx 50$  mol%) were prepared. The water content of the electrolytes was controlled before and after a series of electrochemical measurements.

#### **Electrochemical measurements**

Measuring device:

The electrochemical experiments were performed under ambient pressure and oxygen saturation by means of a ZENNIUM electrochemical workstation (ZAHNER Elektrik GmbH). In the case of [1-EIm][TfO] and [DEMA][TfO], the temperature was varied in the range of 30–90 °C. For [2-SEMA][TfO], the lower

temperature limit had to be increased to 60 °C because, at temperatures < 60 °C and small water contents, the electrolyte solidifies. The heating unit was similar to that described in an earlier publication,<sup>5</sup> but silicon oil was used for heat transfer instead of heating cartridges. The oil temperature was controlled by a LAUDA ECO Gold RE 420GW thermostat. Oxygen saturation in the electrolytes was achieved by purging the gas compartment above the electrolyte with 10 ml/min dry oxygen (99.998% pure), starting 1 hour prior to each series of experiments. The oxygen flow rate was adjusted by means of a Brooks 5850S mass flow controller and a Brooks Microprocessor Control and Read Out Unit 0154. A small cylindrical Pt crucible was used as both the electrolyte vessel and counter electrode.<sup>5</sup> The electrolyte's volume was 3–4 ml. A self-prepared palladium-hydrogen electrode made of a 1 mm Pd wire (99.95%, Goodfellow GmbH) served as a reference electrode.

## *Cyclic voltammograms (CVs):*

Cyclic voltammograms of ORR were recorded using a 7 mm-long Pt wire working electrode with a diameter of 1 mm (99.95%, Goodfellow GmbH) and an actual Pt electrode surface of 0.29 cm². For each experimental condition, 20 consecutive CVs were recorded with a scan rate of 100 mV/s. In order to avoid undesirable Faradaic reactions such as Pt oxidation and H<sub>UPD</sub>, the potential range was limited to 0.3–0.8 V (Pd-H), starting at 0.8 V. The last cycle of each series of CVs was simulated by means of DigiElch 8 from ElchSoft Electrochemical Simulation Software.

## Chronoamperometry:

A home-made disc-shaped microelectrode served as a working electrode for chronoamperometric measurements. A geometric area of 4.9×10<sup>-4</sup> cm<sup>2</sup> was obtained by fusing a 250 µm-thick Pt wire (Heraeus, 99.9%) into Schott AG-Glas<sup>®</sup> glass, then cutting the protruding wire and carefully polishing the tip. The electrical noise due to the small currents was minimized by using a Zahner "HiZ probe" (high impedance probe). The chronoamperometric experiments were begun with a potential step from OCV to the potential range of the limiting current. The resulting *i/t*-curves were analyzed by means of the Shoup/Szabo<sup>35</sup> equation in order to obtain diffusion coefficients and concentrations of oxygen in PIL/water mixtures.

Water uptake experiment:

The water uptake experiment of [1-EIm][TfO] was performed under similar conditions as those described for [2-SEMA][TfO] and [Dema][TfO]. A volume of  $\approx 5$  ml of [1-EIm][TfO] was exposed in an open glass vessel to ambient atmosphere over a period of 8422 h and the weight was measured at regular intervals. The volume-to-surface ratio was  $\approx 1$  cm. The average values of the temperature, relative humidity and thus of the water vapor's partial pressure were  $(21.7 \pm 0.8)$  °C,  $(32.0 \pm 5.8)$ % and  $(841 \pm 164)$  Pa.

## RESULTS AND DISCUSSION

## **ORR** mechanism and input parameters

Before running the simulation of the cyclic voltammograms with DigiElch 8, the input of a (proper) reaction mechanism is required. Broadly speaking, three ORR mechanisms can be distinguished (see *e.g.*, Katsounaros et al.<sup>36</sup>): (i) A dissociative mechanism, (ii) a peroxo mechanism and (iii) an associative mechanism. A scheme of these mechanisms, adopted from Katsounaros et al., is shown in Figure 2.

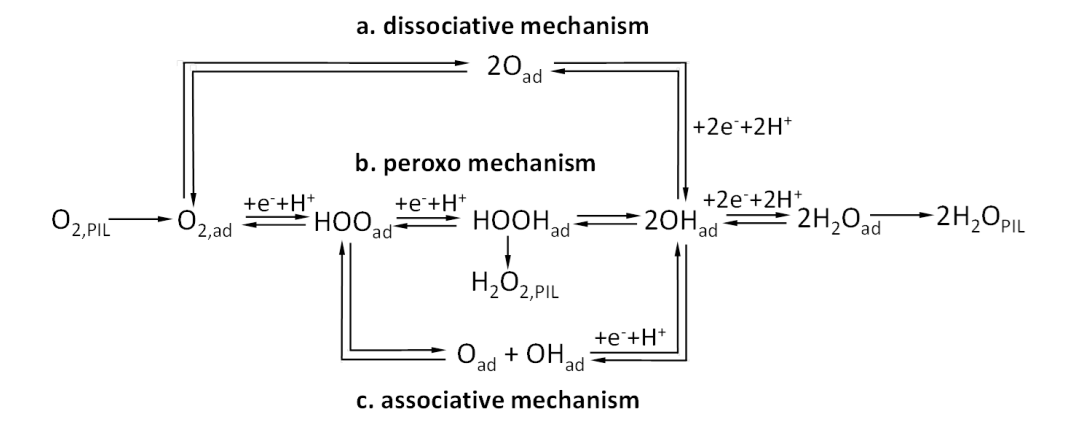


Figure 2. Scheme of possible ORR mechanisms, adapted from Katsounaros et al.<sup>36</sup>

For fuel cell applications, a four-electron mechanism with water as the main reaction product is essential. A substantial amount of the oxygen that reacts through a two-electron mechanism would considerably decrease the performance. Moreover, the generated H<sub>2</sub>O<sub>2</sub> may form hydroperoxyl radicals (HO<sub>2</sub>•) that would attack and degrade the polymer membrane<sup>37-38</sup> (*e.g.*, PBI or Nafion®). Indeed, several PILs revealed a 4 e<sup>-</sup> ORR mechanism on Pt, such as [DEMA][TfO],<sup>6,39</sup> fluorohydrogenated ionic liquids like EMPyr(FH)<sub>1.7</sub>F<sup>18</sup> and [2-SEMA][TfO],<sup>6</sup> whereas others like ethylammonium nitrate (EAN) or bis-(2-methoxyethyl)ammonium sulfamate [(MeOEt)<sub>2</sub>NH][OSA] showed an irreversible two-electron ECEC mechanism.<sup>40</sup>

The total number n of transferred electrons can be estimated from the limiting ORR current density if the bulk parameters of the electrolyte, such as the diffusion coefficient and the concentration of oxygen, are known. In the case of [1-EIm][TfO], the measurements of the ORR limiting current on a Pt micro-disc electrode revealed a number of transferred electrons of  $n \approx 5$  (see Figure S1 in the Supporting Information). The deviation from the expected n value of 4 is mainly due to the error in the determination of the mass transport parameters. In the case of [DEMA][TfO] and [2-SEMA][TfO], n values of about 4 were calculated from limiting diffusion current densities in RDE experiments. RRDE measurements revealed a negligible production of  $H_2O_2$  on Pt in [DEMA][TfO], thus confirming  $n \approx 4.39$  This does not, of course, exclude the formation of small amounts of  $H_2O_2$ .

The reaction order m of the ORR with respect to the concentration of molecular oxygen should be 0.5 in the case of the dissociative mechanism (first electron transfer to adsorbed oxygen atoms), but 1 for the associative and peroxo mechanisms, where the molecular oxygen is reduced in the r.d.s. Recently published experiments with a hanging meniscus Pt disc RDE (HMRDE) in contact with [2-SEMA][TfO]<sup>6</sup> were analyzed in terms of the reaction order by plotting  $\log i \ vs. \log [1-(i/i_{lim})]$  for various rotation rates and potentials.<sup>41</sup> Reaction orders of about 1 were obtained, as can be seen in Figure S2a (see the Supporting Information). The same is true for [1-EIm][TfO] and [DEMA][TfO], where the slope m was calculated from

double-logarithmic plots of  $j_k$  vs. oxygen concentration (see Figure S2b in the Supporting Information). Hence, the dissociative mechanism can be excluded here.

The residual errors when fitting a model with the associative mechanism were always somewhat smaller compared to a model with the peroxo mechanism. A clear distinction of these two mechanisms is not possible on the basis of these experimental results. However, this is not a crucial point, because the rate-determining step, the first electron transfer, is identical for both mechanisms. Thus, the simulated key parameters of the r.d.s.,  $E_{01}$ ,  $\alpha_1$ , and  $k_1$  are also almost identical. Moreover,  $H_2O_2$  generated in a dominant peroxo mechanism should desorb from the Pt surface to a certain extent and lead to a decrease in the overall number of transferred electrons, which is not observed. For this reason and because the associative mechanism is widely accepted and has been proposed for ORR on Pt in diluted and concentrated acid solutions,  $^{42-43}$  as well as ionic liquids,  $^{44}$  only the associative mechanism was used for the simulations with DigiElch 8.

In addition, the proton-donating species must be specified. In particular,  $H_3O^+$  must be considered, which is formed in the protolysis equilibrium of BH<sup>+</sup> and H<sub>2</sub>O. The H<sub>UPD</sub> experiments revealed that the extrapolated H<sub>UPD</sub> charge in water-free [2-SEMA][TfO] amounts to only 9.4% of the maximum H<sub>UPD</sub> charge (210  $\mu$ C/cm<sup>2</sup>), whereas that in the water-free [DEMA][TfO] is only 1.8%.<sup>14</sup> This suggests that H<sub>3</sub>O<sup>+</sup> is a much better proton donator in H<sub>UPD</sub> compared to BH<sup>+</sup>. When comparing the pK<sub>a</sub> values (valid for diluted aqueous solutions) of H<sub>3</sub>O<sup>+</sup>(0), [DEMA]<sup>+</sup> (10.55) and [2-SEMA]<sup>+</sup> (0.94), it is evident that [DEMA]<sup>+</sup> has by far the lowest proton-donating ability, whereas that of [2-SEMA]<sup>+</sup> and H<sub>3</sub>O<sup>+</sup> should be comparable. An advantage of [2-SEMA]<sup>+</sup> over H<sub>3</sub>O<sup>+</sup> has several orders of magnitude higher concentration. On the other hand, a steric hindrance of the proton transfer and/or poor accessibility to the Pt surface might be a disadvantage of [2-SEMA]<sup>+</sup>. The far higher BH<sup>+</sup> concentration is the only difference in the input values when simulating CVs with either an ORR mechanism via BH<sup>+</sup> or H<sub>3</sub>O<sup>+</sup>. Fortunately, the influence of the type of proton donator on the key parameters of the r.d.s. turned out to be small and simulations with ORR mechanisms via BH<sup>+</sup> and H<sub>3</sub>O<sup>+</sup> yield similar results (as an example, see Figure S3 in the Supporting

Information). For the afore-mentioned reasons and the fact that only PIL/water mixtures were used here, which guarantees the presence of  $H_3O^+$ , with the following associative ORR mechanism with  $H_3O^+$  as the proton donating species being used for all of the simulations:

Apart from the ORR reaction mechanism, the input of fixed parameters such as the physico-chemical properties and starting values for the variables of the partial reaction steps is required. Amongst the fixed parameters, the bulk concentration and bulk diffusion coefficient of oxygen have by far the greatest impact on the fit results. The  $D_{02}$  and  $c_{02}$  values for PIL/water mixtures of [DEMA][TfO], [1-EIm][TfO] and [2-SEMA][TfO] were obtained according to the procedure and experimental conditions described in the experimental part. Then, the polynomial fits of the semi-logarithmic plots of  $D_{02}$  and  $c_{02}$  vs.  $\log(x_{\rm H2O})$  for different temperatures were performed (see figures S4/S5 in the Supporting Information). Finally, the  $D_{02}$  and  $c_{02}$  values for the water concentrations used in the ORR experiments were calculated from the polynomial equations and entered as input values for the simulation of the CVs (see tables 1 and 2). Moreover, the  $D_{02}$  and  $c_{02}$  values, bulk concentrations of  $H_3O^+$  and  $H_2O$  were calculated (see tables S1 and S2 in the Supporting Information).

The ORR measurements were simulated by assuming the Butler-Volmer (B-V) model to describe the underlying charge transfer processes. Thus, the starting values of the variables of the B-V equation were entered for each partial step, *i.e.*, equilibrium potentials,  $E_0$ , charge transfer coefficients,  $\alpha_1$ , and rate

constants, k. The fit results reveal a dominating influence of the variables of the first electron transfer step (see Eq. 3a), therefore confirming this partial step as rate-determining. In the following, particular attention is paid to the rate constant of the first step,  $k_1$ , which dominates the overall performance of the ORR, depending on the PIL acidity, water content and temperature.

Table 1.  $D_{O_2}$  values for [DEMA][TfO], [1-EIm][TfO] and [2-SEMA][TfO] at the experimental conditions of the cyclic voltammograms; data is taken from the fit curves in Figure S1a.

PIL	10 <sup>5</sup> D <sub>O2</sub> / cm <sup>2</sup> s <sup>-1</sup>						
[DEMA][TfO]	x <sub>H2O</sub> / mol%	T/°C					
		30	50	70	90		
	5.0	0.39	0.47	0.55	0.63		
	11.4	0.43	0.53	0.64	0.74		
	22.9	0.50	0.64	0.78	0.92		
	35.1	0.57	0.76	0.94	1.12		
	50.0	0.68	0.92	1.17	1.41		
_ [1-Elm][TfO]	x <sub>H2O</sub> / mol%	T/°C					
		30	50	70	90		
	2.8	0.36	0.64	1.04	1.54		
	14.4	0.42	0.69	1.11	1.68		
	23.3	0.48	0.76	1.21	1.83		
	36.2	0.56	0.87	1.37	2.06		
	48.3	0.64	0.99	1.55	2.30		
[2-SEMA][TfO]	<i>x</i> <sub>H2O</sub> / mol%	T/°C					
		60	70	80	90		
	11.7	0.15	0.15	0.18	0.26		
	21.3	0.14	0.15	0.18	0.25		
	33.6	0.16	0.18	0.20	0.28		
	40.3	0.17	0.20	0.23	0.30		
	48.3	0.20	0.23	0.26	0.35		
	52.7	0.22	0.25	0.29	0.38		

Table 2.  $C_{O_2}$  values for [DEMA][TfO], [1-EIm][TfO] and [2-SEMA][TfO] at the experimental conditions of the cyclic voltammograms; data taken from the fit curves in Figure S1b.

PIL	10 <sup>6</sup> c <sub>O2</sub> / mol cm <sup>-3</sup>							
[DEMA][TfO]	<i>x</i> <sub>H2O</sub> / mol%	T/°C						
		30	50	70	90			
	5.0	2.45	4.12	5.73	7.33			
	11.4	2.79	4.00	5.13	6.25			
	22.9	2.88	3.64	4.34	5.02			
	35.1	2.82	3.28	3.72	4.13			
	50.0	2.64	2.86	3.09	3.29			
[1-Elm][TfO]	x <sub>H2O</sub> / mol%	T/°C						
		30	50	70	90			
	2.8	2.40	2.34	2.28	2.23			
	14.4	2.70	2.52	2.34	2.14			
	23.3	2.65	2.45	2.23	2.01			
	36.2	2.52	2.30	2.07	1.83			
	48.3	2.38	2.15	1.92	1.68			
[2-SEMA][TfO]	<i>x</i> <sub>H2O</sub> / mol%	T/°C						
		60	70	80	90			
	11.7	0.63	0.85	1.03	1.24			
	21.3	0.73	0.90	1.06	1.23			
	33.6	0.80	0.93	1.07	1.20			
	40.3	0.84	0.94	1.07	1.19			
	48.3	0.87	0.95	1.06	1.16			
	52.7	0.88	0.95	1.06	1.15			

# Influence of the water content

Figure 3 shows the typical CVs of the three PILs for a temperature of 90 °C and a water content of about 4 wt% ( $\approx$  35–40 mol%). The simulated curves (solid lines) match the measured data (dashed lines) quite well. Clearly, there are significant differences between the CVs of the low-acidic PILs ([DEMA][TfO]/[1-EIm][TfO]) and that of the strong acidic PIL [2-SEMA][TfO]. In the presence of [2-SEMA][TfO], the onset potential of the ORR shifts by about 150 mV to more positive values. This leads to a much higher ORR current density at the electrode potentials > 0.4 V, *i.e.*, a potential range that is relevant for fuel cell cathode

operation. Below 0.4 V, [DEMA][TfO] and [1-EIm][TfO] yield significantly higher ORR current densities, which can be explained by faster oxygen transport. This is supported by the  $D_{02} \cdot c_{02}$  values of [DEMA][TfO]  $(4.6 \cdot 10^{-11} \text{ mol cm}^{-1} \text{ s}^{-1})$  and [1-EIm][TfO],  $(3.8 \cdot 10^{-11} \text{ mol cm}^{-1} \text{ s}^{-1})$ , which are more than one order of magnitude higher than those of [2-SEMA][TfO]  $(3.6 \cdot 10^{-12} \text{ mol cm}^{-1} \text{ s}^{-1})$ , see tables 1 and 2) at the conditions as described in Figure 3. In general, the potential range of the ORR limiting current is reached at potentials  $\leq -0.1$  V for [DEMA][TfO] and [1-EIm][TfO], but at much greater positive potentials  $\leq 0.4$  V in the case of [2-SEMA][TfO].

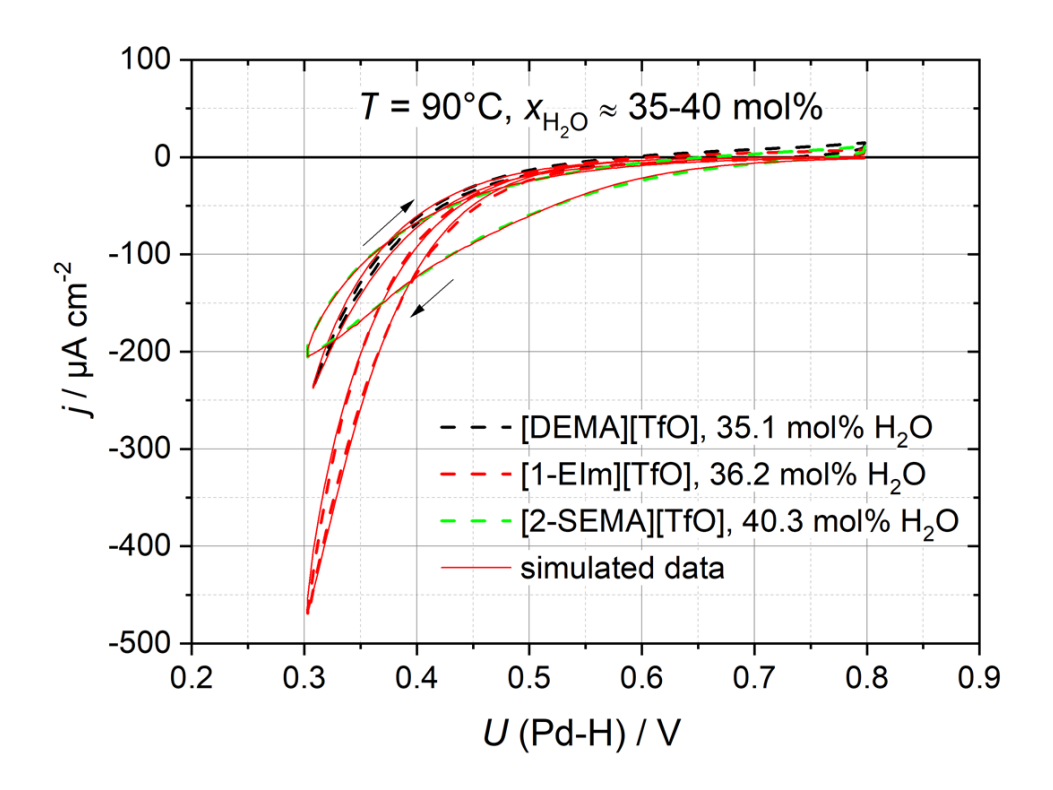


Figure 3. Cyclic voltammograms (broken lines) and simulated data (full red lines) of ORR on Pt in PIL/water electrolytes as a function of the water content; a comparison of [DEMA][TfO], [1-EIm][TfO] and [2-SEMA][TfO] to the examples of  $T = 90^{\circ}C$  and 35-40 mol%  $H_2O$ .

Another feature of [2-SEMA][TfO] is a larger hysteresis of the forward and backward scans. One explanation is the slow pseudo-capacitive processes such as the specific adsorption of ions on the catalyst surface, which causes a hysteresis in the double layer capacitance.<sup>45</sup> Slow pseudo-capacitive processes would also mean a (too) slow change in the coverage of ions, water, oxygen, and oxygen intermediates on

the Pt surface during the CV and thus a change in the ORR current density at the same potentials in the forward and backward scans. Although the interaction of sulfonates with the Pt surface is relatively small compared to halides or phosphate, <sup>46</sup> a stronger adsorption of the [2-SEMA]<sup>+</sup> on Pt due to the sulfonate group would explain the larger hysteresis as well. Generally speaking, the BH<sup>+</sup> concentration on the Pt surface should increase with decreasing potential (and vice versa) for electrostatic reasons. Oxygen diffusion limitation may also play a role: at the lower potential limit of 0.3 V, the ORR current density in the presence of [2-SEMA][TfO] is close to or within the limiting current regime. This is different in the case of [DEMA][TfO] and [1-EIm][TfO], where only current densities in the mixed kinetic and mass transport-controlled regime are achieved at 0.3 V. Providing that the surface concentration of oxygen and thus the concentration profile in a growing Nernstian diffusion layer changes only slowly (see above), a hysteresis must occur.

The influence of the water content on the ORR kinetics on Pt in the presence of PILs with different acidities is shown in Figure 4a-c for a temperature of 70 °C. The quality of most of the fits is good, and the fitting errors are less than 3%. Larger deviations only occur at low current densities, where unavoidable (pseudo-) capacitive processes play a role. If  $H_3O^+$  is the dominating proton donator (see Eq. 3b), one would expect an increase in the ORR current with increasing water content, because the  $H_3O^+$  concentration increases as well. [DEMA][TfO] and [1-EIm][TfO] meet this expectation, whereas [2-SEMA][TfO] shows anomalous behavior with a distinct minimum at medium water contents of about 20–30 mol%. The latter effect has been found in HMRDE experiments<sup>6</sup> and impedance measurements, <sup>15</sup> too (see Figure S6 in the Supporting Information). The pseudo-capacitance  $C_2$  of [2-SEMA][TfO], derived from the impedance measurements, is especially interesting, as it is the only interfacial (or bulk) parameter which—apart from the current density or rate constant of ORR—shows a minimum water content of about 30 mol%.

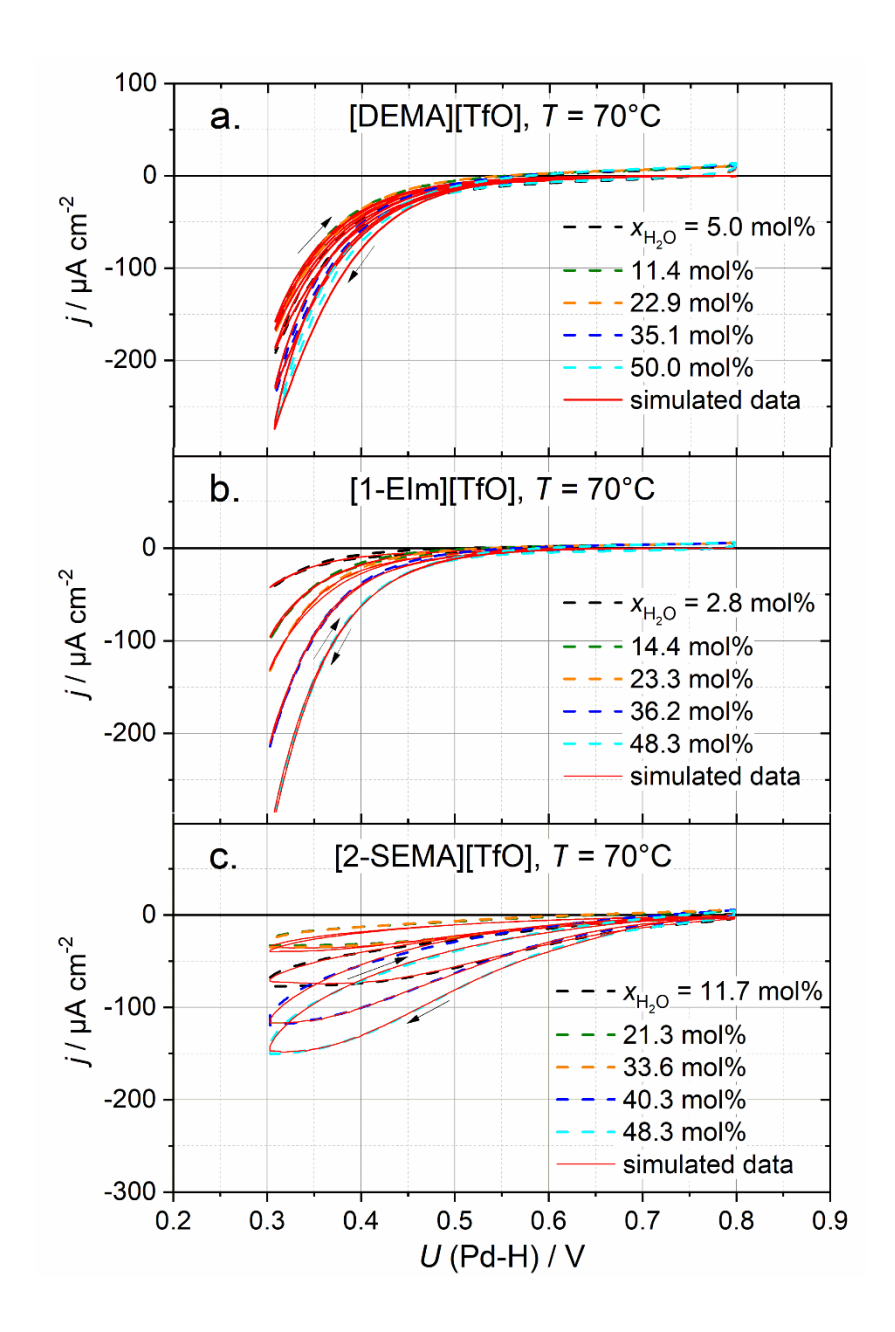
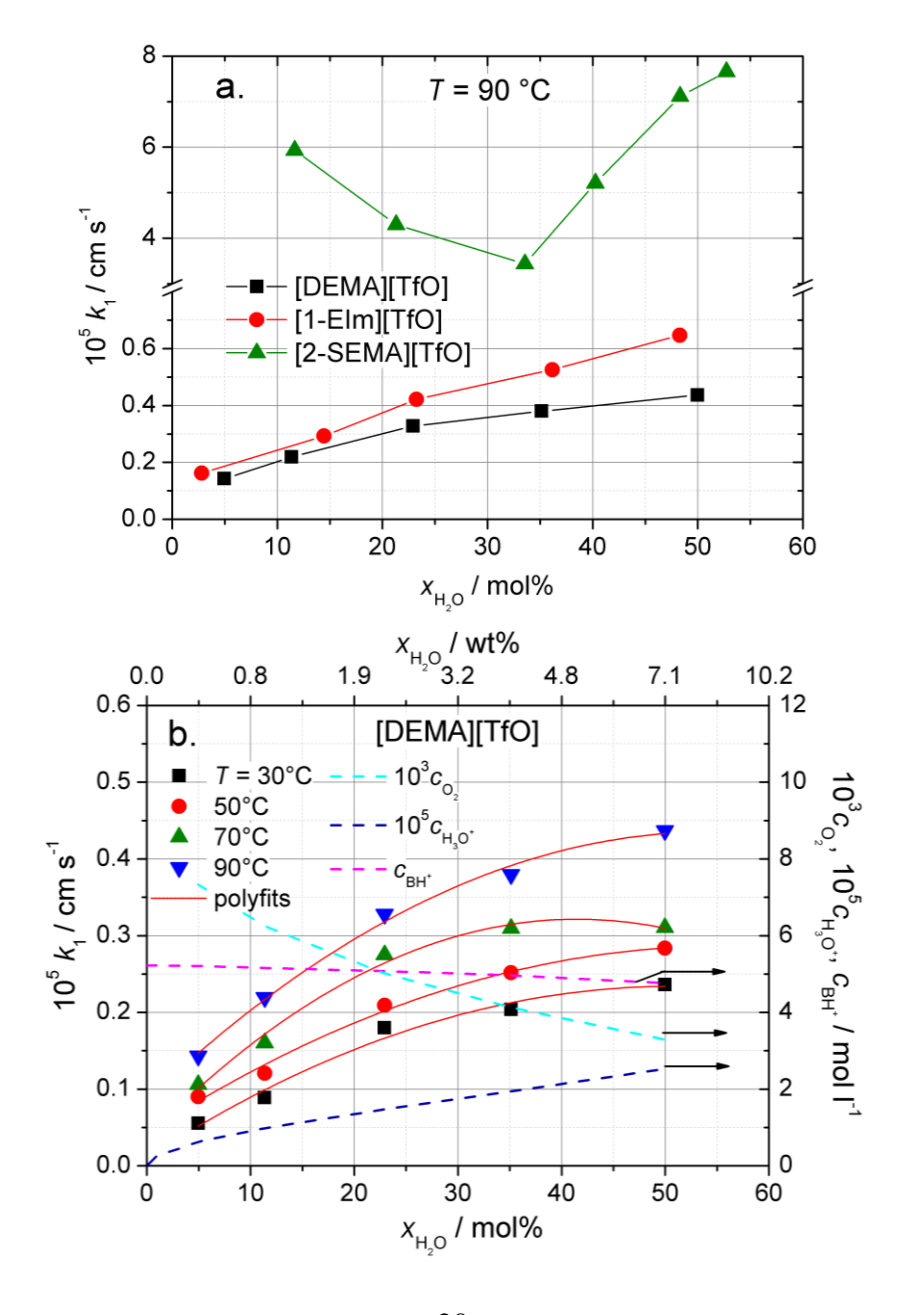


Figure 4. CVs (broken lines) and simulated data (full red lines) of ORR on Pt for a. [DEMA][TfO], b. [1-EIm][TfO] and c. [2-SEMA][TfO] at various water contents for the example of T = 70 °C.

To gain a better understanding of these results, the dependence of the rate constant  $k_1$  (r.d.s., see Eq. 3a) on the water content was investigated in more detail. Fig. 5a shows a comparison of these dependencies for a temperature of 90 °C. Clearly,  $k_1$  reveals a similar dependence on the water content to the overall current density, which confirms the assumption that the first electron transfer is the rate-determining step.

Another important result is the increase in  $k_1$  with the increasing acidity of the cation. According to the onset potentials of the ORR current resulting from Figure 3, the  $k_1$  values of [2-SEMA][TfO] are more than one order of magnitude higher than those of [DEMA][TfO] and [1-EIm][TfO], whereas the latter only slightly differ. The complete results of  $k_1$  for the three PILs and the entire investigated temperature range are depicted in Figure 5b-d. In order to compare the dependence of  $k_1$  on the water content with that of ORR educts, the concentrations of oxygen,  $H_3O^+$  and  $BH^+$  are also presented (see the dashed lines). Note that the educt concentrations are shown for 90 °C.



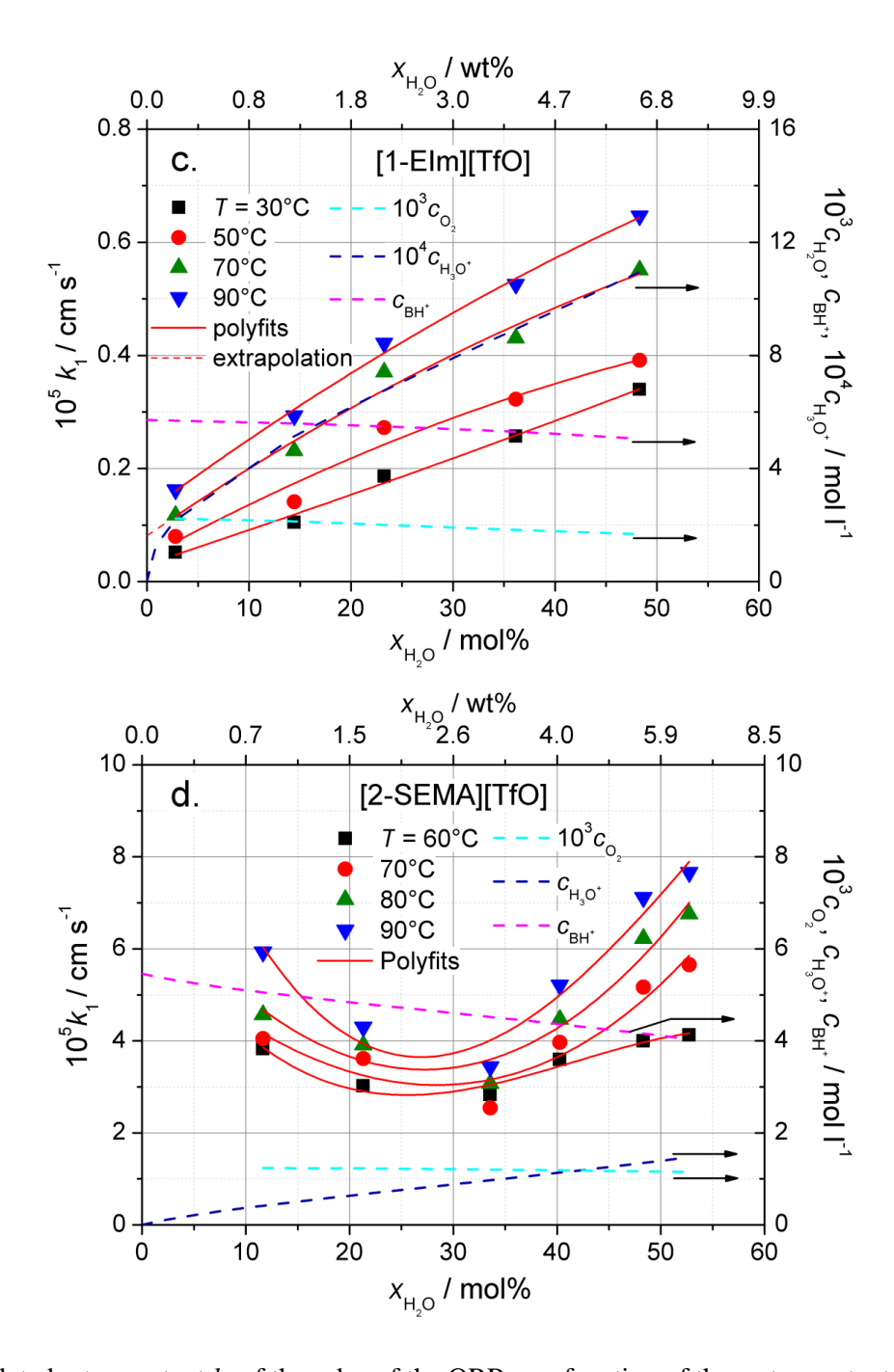


Figure 5. Simulated rate constant  $k_1$  of the r.d.s. of the ORR as a function of the water content; a.: comparison of [DEMA][TfO], [1-EIm][TfO] and [2-SEMA][TfO] for the example of T = 90 °C; b.-d.: plots of  $k_1$  vs. the water content for the three PILs at various temperatures; on the right axis, the concentrations of oxygen,  $H_3O^+$  and cations are plotted as well; the polynomial fits (full red lines) only serve as a visual guide.

Because the temperature dependence of these parameters is small, the concentration profiles for the other investigated temperatures are very similar. The polynomial fits of  $k_1$  vs.  $x_{\rm H2O}$  have no physical meaning and merely serve as a visual guide. An increase of  $k_1$  with increasing temperature is expected due to the thermal activation of the ORR. In the case of [DEMA][TfO] and [1-EIm][TfO], the course of the curves of  $k_1$  are similar to that of  $c_{\rm H3O+}$ , which suggests a correlation of these parameters. In contrast, the decreasing  $O_2$  and  $O_2$  and  $O_3$  and  $O_4$  concentrations indicate that they do not have a significant influence on  $O_4$ . The similarity of the  $O_4$  and  $O_4$  courses becomes especially apparent in Figure 5c where, by chance, the courses of the  $O_4$  curve at 70 °C and of the  $O_4$  curve fully coincide. This example suggests that following the course of the  $O_4$  curve,  $O_4$  could potentially achieve a very small value of close to nil as the water concentration approaches zero. On the other hand, the extrapolation of the polynomial fit to  $O_4$  (see red dashed line) would yield an incorrect, too high of a value for  $O_4$ .

Although  $H_3O^+$  is not involved in the rate-determining electron transfer step (Eq. 3a), a sufficient surface concentration of a good proton donator is required to enable the fast reaction of the oxygen intermediates formed in the ORR partial steps (see eqs. 3b, 3e and 3g). Clearly, the [DEMA]<sup>+</sup> and [1-EIm]<sup>+</sup> cations are bad proton donators because of their very low acidity levels. This means that if the water and so the  $H_3O^+$  concentrations are too small, the proton transfer would also become rate-determining as well. In the case of the acidic [2-SEMA][TfO], the situation is different and more complex. Even though  $H_3O^+$  would be the more effective proton donator compared to the [2-SEMA]<sup>+</sup> cation, it must not be forgotten that the [2-SEMA]<sup>+</sup> cation is strongly acidic and its concentration is more than one order of magnitude higher at a water content lower than 20 mol%. These properties explain a rate constant  $k_1$  at  $x_{H2O}$ =0 that is significantly higher than the corresponding  $k_1$  values in the presence of [DEMA][TfO] and [1-EIm][TfO]. Because of the strong hygroscopicity of the PILs, especially of [2-SEMA][TfO], the  $k_1$  values could not be determined at very low water contents. However, a dramatic drop of  $k_1$  in the (ideally) neat ionic liquid seems fairly improbable, *i.e.*, it is likely that  $k_1$  is higher at  $x_{H2O}$ =0 than at 20 mol% of water. Thus, in accordance with these considerations, the [2-SEMA]<sup>+</sup> cation must be a better proton donator for the ORR as assumed only on the basis of the  $H_{UPD}$  measurements (see above). This result is notable because the Pt surface charge is

less positive or even negative at low  $(H_{UPD})$  potentials. Thus, the surface coverage of [2-SEMA]<sup>+</sup> cations and their availability as proton donators should be higher in the  $H_{UPD}$  region.

If a poisoning or blocking effect were the cause of the low H<sub>UPD</sub> charge but enhanced ORR rate at low water concentrations, the potential of zero charge (PZC) must be considered. This is because the PZC determines the sign and value of the Pt surface charge and therefore the sign and concentration of ions on the Pt surface and in the innermost layer of the electrolyte at a certain potential. Unfortunately, the PZC is not known for [2-SEMA][TfO] and the PIL/water mixtures investigated here. For platinum in aqueous solutions, a PZC of around 0.3 V / NHE has been established.<sup>47</sup> A similar value was found for neat [DEMA][TfO] (0.271 V). <sup>16</sup> If [2-SEMA][TfO] would have a similar PZC, the charge of the Pt surface would be strongly positive in the ORR potential region (e.g., 0.8 V), but small or even negative in the H<sub>UPD</sub> region. Because [TfO] anions would be strongly adsorbed in the ORR region, but less adsorbed in the H<sub>UPD</sub> region, they can be excluded as the reason for a possible blocking effect. Moreover, it is known from aqueous solutions that [TfO]<sup>-</sup> does not specifically adsorb (chemisorb) on the Pt surface.<sup>48</sup> Conversely, [2-SEMA]<sup>+</sup> cations in particular would be adsorbed in the H<sub>UPD</sub> region. However, after the proton transfer to the Pt surface and its reduction to H<sub>ad</sub>, the proton donator [2-SEMA]<sup>+</sup> will be converted to the conjugated base, Nmethyltaurine. A blocking or poisoning of adsorption sites by large, neutral N-methyltaurine molecules would explain the small surface coverage of H<sub>ad</sub>. In fact, a poisoning effect in the H<sub>UPD</sub> region by the conjugated base diethylmethylamine in the case of [DEMA][TfO] has been reported by Goodwin et al.<sup>49</sup> In contrast to the conjugated base in Goodwin's work, the concentration of the conjugated base Nmethyltaurine (0.4–1.5 mol/L) is many orders of magnitude higher. Thus, a poisoning of the Pt surface by neutral N-methyltaurine bulk molecules should be a general issue. However, in the ORR potential region, the access of the large N-methyltaurine molecules to the Pt surface will be largely blocked by [TfO], whereas in the H<sub>UPD</sub> region close to the PZC, a blocking effect by bulk molecules is quite possible. A final answer to the question of whether or not the conjugated base N-methyltaurine has a poisoning or blocking effect in the H<sub>UPD</sub> region cannot be given and requires further experiments, including the determination of the PZC and the investigation of adsorbates, e.g., by spectroscopic methods and AFM.

Generally, a dependence of  $k_1$  on the concentration of the proton donator should always lead to a minimum: if the water concentration approaches zero, the  $H_3O^+$  concentration becomes too small to maintain the ORR current and the PIL cation must take over the function of a proton donator. Because the BH<sup>+</sup> concentration increases with decreasing water content,  $k_1$  must increase when approaching  $x_{H2O} = 0$ . In the case of [DEMA][TfO] and [1-EIm][TfO], where the acidity of the cations is many orders of magnitude lower than that of  $H_3O^+$ , the minimum should occur close to  $x_{H2O} = 0$ . This is different from the acidic [2-SEMA][TfO], where the minimum appears at a much higher water content. However, these considerations do not explain the steep decrease of  $k_1$  at water contents below 20 mol%.

# **Influence of temperature**

The activation energies and pre-exponential factors of  $k_1$  may provide further, valuable information on the influence of the PIL acidity and water content on the rate constant. Therefore, temperature-dependent CVs were recorded and simulated by means of the DigiElch software. Figure **6**a-c shows the measured and fitted CVs in a temperature range of 30–90 °C ([DEMA][TfO]/[1-EIm][TfO]) and 60–90 °C ([2-SEMA][TfO]), respectively, for the example of a water content of  $(22 \pm 1)$  mol%.

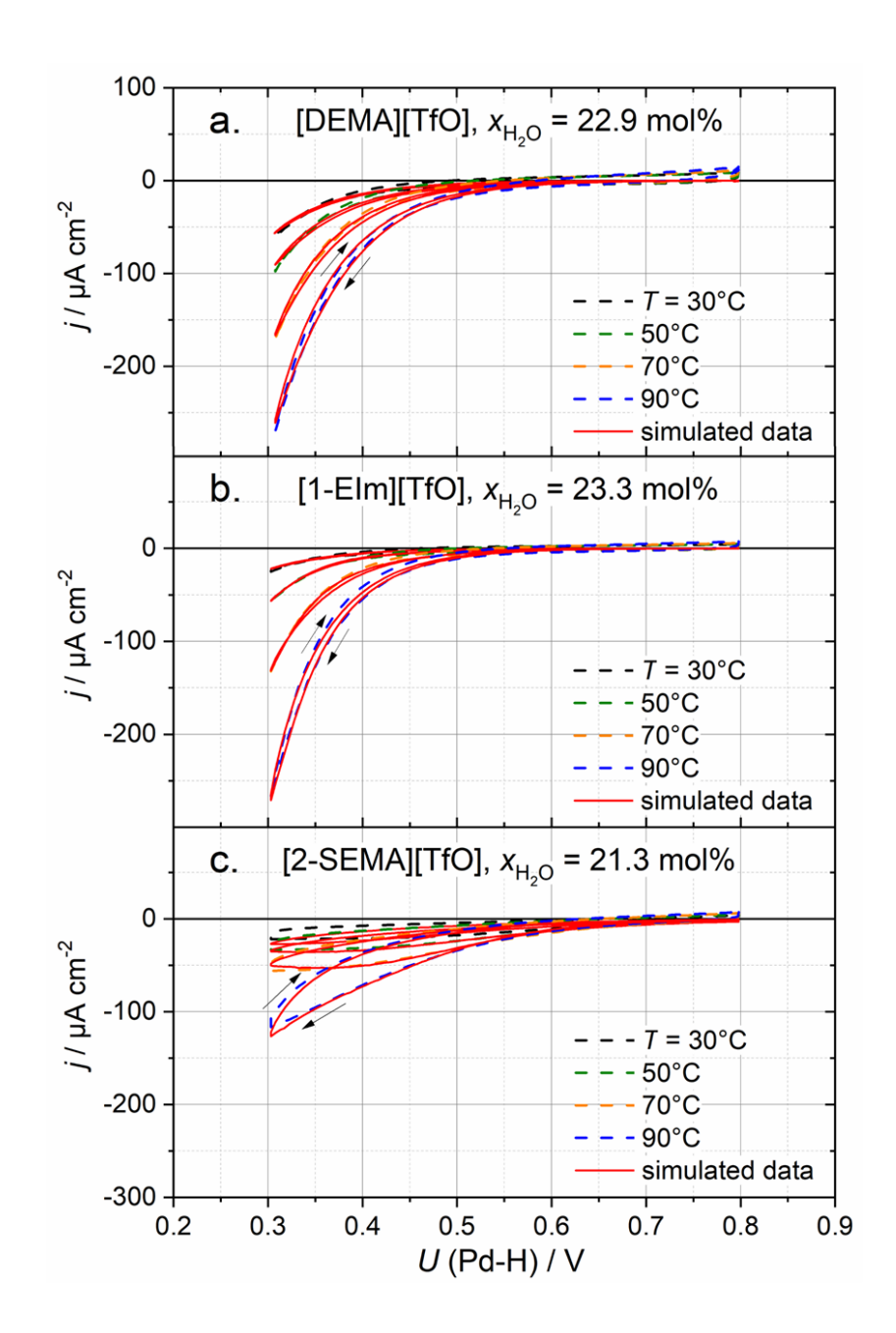
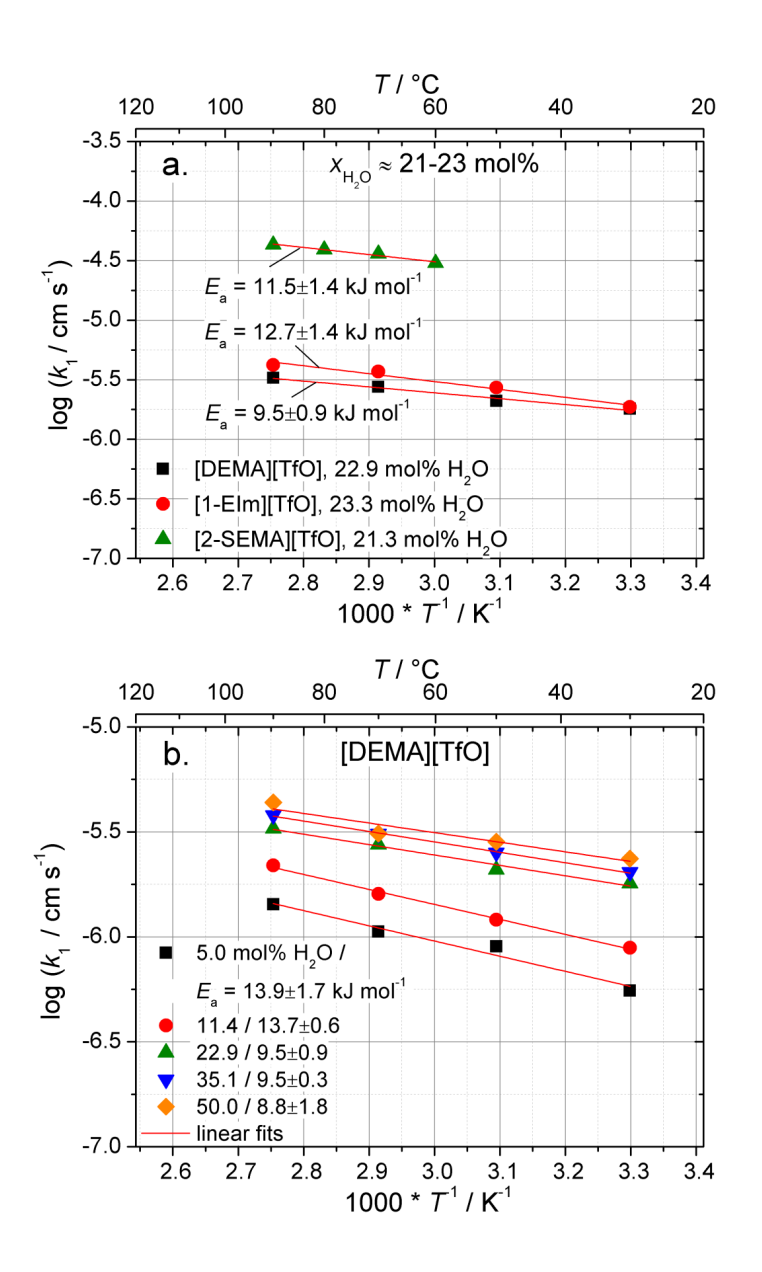


Figure 6. CVs (broken lines) and simulated data (full red lines) of ORR on Pt for a. [DEMA][TfO], b. [1-EIm][TfO] and c. [2-SEMA][TfO] at various temperatures for the example of a water content of  $\approx$ 21-23 mol%.

The temperature dependencies of the  $k_1$  values of all three PILs exhibit a distinct Arrhenius behavior, as demonstrated in Figure 7. Figure 7a shows a comparison of Arrhenius plots for the three PILs for the above-mentioned water concentration. While the  $k_1$  values of [2-SEMA][TfO]/water mixtures are about ten times

higher than those of [DEMA][TfO] and [1-EIm][TfO], the activation energies are fairly similar and situated within a range of about 10 to 13 kJ/mol. Activation energies in the range of 7–20 kJ/mol are also obtained for the other investigated water contents (see Figure 7b-d).



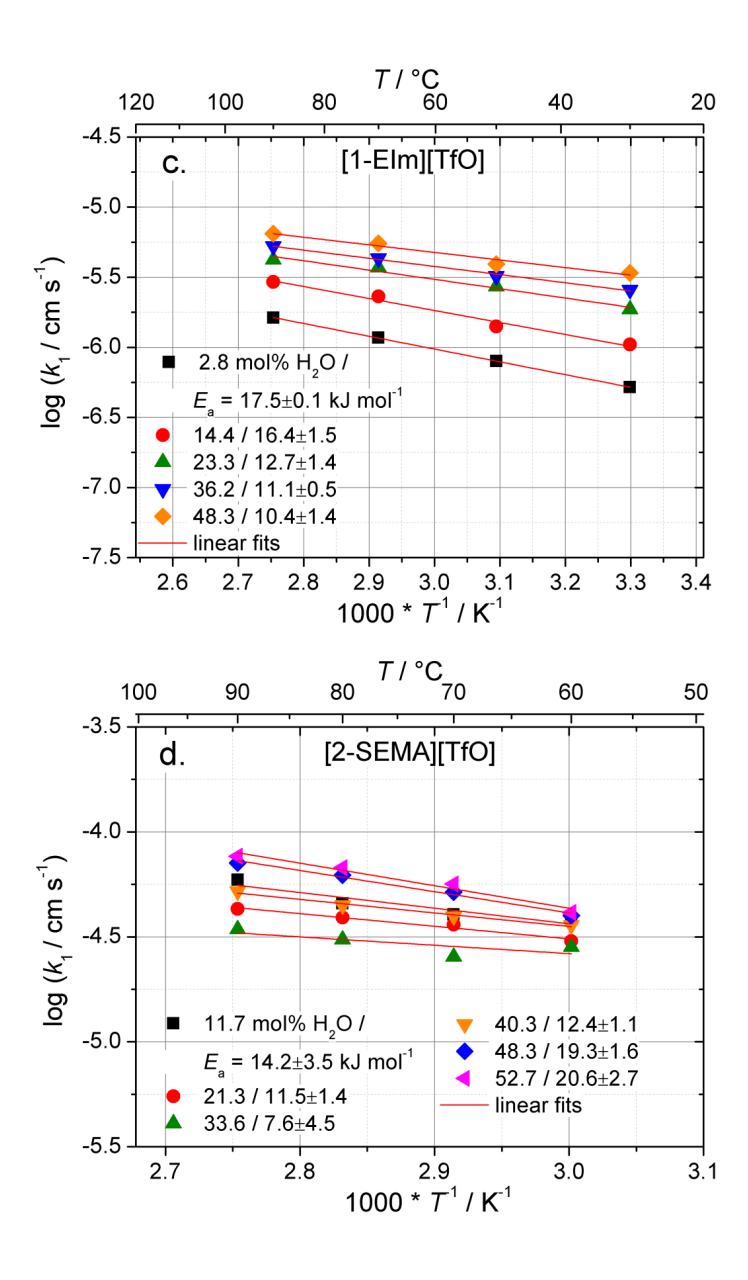


Figure 7. Arrhenius plots of  $k_1$ ; a.: comparison of [DEMA][TfO], [1-EIm][TfO] and [2-SEMA][TfO] for the example of  $x_{H2O} \approx 21-23$  mol%; b.-d.: Arrhenius plots of  $k_1$  for the three PILs with various water contents.

Unfortunately, the activation energies of  $k_1$  are difficult to find in the literature. Nevertheless, comparable activation energies of the ORR current density of about 18–20 kJ/mol have been reported by Khan et al.<sup>40</sup> for various PILs. Figure 8 shows similar dependencies of the activation energies and pre-exponential factors of  $k_1$  on the water content. This corresponds to the well-known compensation effect that is widely found in (electro-)catalytic processes and which is based on a linear relationship of activation

enthalpy and entropy.<sup>50-51</sup> Up to a water content of  $\approx$  35 mol%, the activation energies for the three PILs are similar and tend to decrease. This result supports the assumption that the same ORR mechanism and rate-determining step is valid for the PILs, regardless of their acidity. It is probable that water molecules are involved in the activated complex and influence both the activation energy and entropy. At higher water contents,  $E_a$  increases in the case of [2-SEMA][TfO], but remains almost constant for [DEMA][TfO] and [1-EIm][TfO]. Ultimately, the latter values will increase at higher water contents as well, because the activation energies of the ORR on Pt in aqueous solutions (or in contact with water-containing polymers like Nafion®) are in the range of about 40–50 kJ/mol.,<sup>40, 52</sup> and are thus substantially higher than those obtained with the PILs.

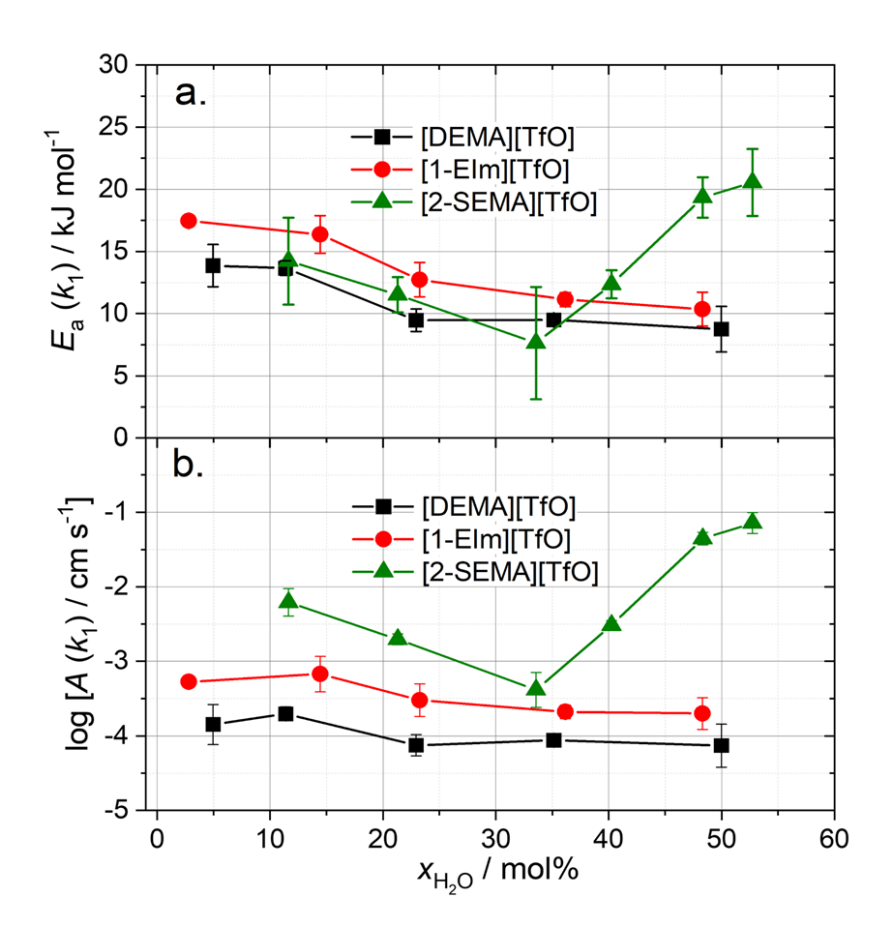


Figure 8. Activation energy (a.) and pre-exponential factor (b.) of  $k_1$  derived from the linear fits of the Arrhenius plots shown in Figure 7.

A probable explanation may relate to the additional hydration enthalpies and entropies of the reactants and activated complex, which should be considered at higher water contents. The increase in the  $E_a(k_1)$  of [2-SEMA][TfO], even at about 35 mol% of water, suggests a higher degree of hydration of ions on the Pt surface and in the double layer (at the same bulk water content) compared to [DEMA][TfO] and [1-EIm][TfO]. This assumption corresponds to the strong hygroscopicity and six-fold higher water uptake of [2-SEMA][TfO] mentioned above. In the PIL/water mixtures of [DEMA][TfO] and [1-EIm][TfO],  $k_1$  increases with the water content. Because the decrease in the pre-exponential factor provokes the opposite behavior, the simultaneous decrease in activation energy must be the dominating effect. The reverse is true for [2-SEMA][TfO], where the pre-exponential factor determines the V-shaped plot of  $k_1$  vs. vs. This result may be interpreted such that the activation entropy plays an important role in the r.d.s. for [2-SEMA][TfO], whereas the activation enthalpy seems to be more important for the less acidic and less hygroscopic PILs.

In addition to the water content, the acidity of the PIL cations is also important, which is reflected in the decrease in the pre-exponential factor by 1–3 orders of magnitude with increasing  $pK_a$ , *i.e.*, in the order [2-SEMA][TfO] > [1-EIm][TfO] > [DEMA][TfO]. Clearly, the pre-exponential factor increases with increasing acidity and surface concentration of the proton donators. On the one hand, the  $pK_a$  values (valid for diluted aqueous solutions) are only rough estimates for the acidity of the PIL cations and, moreover, might change under the influence of the electric field of the double layer. On the other hand, the acidity of [2-SEMA]<sup>+</sup> is by  $\approx 7$  to 10 orders of magnitude higher than that of [1-EIm]<sup>+</sup> and [DEMA]<sup>+</sup>, and the bulk concentration of H<sub>3</sub>O<sup>+</sup> in [2-SEMA][TfO]/water mixtures should be 3–5 orders of magnitude higher compared to [1-EIm][TfO] and [DEMA][TfO] (see Table S1 in the Supporting Information). For these reasons, it is likely that the bulk values of acidity and proton concentration are reflected in surface properties like surface coverage, orientation and the bonding of ions, water molecules and oxygen (intermediates), which affect the pre-exponential factor regarding the activation entropy and number of active surface sites.

Although the question of why [2-SEMA][TfO] shows a distinct minimum when plotting  $k_1$  vs. the water content cannot be answered conclusively, some tentative explanations can be given on the basis of the aforementioned results:

- (i) At small and increasing water contents, [2-SEMA]<sup>+</sup> cations in the innermost layer are increasingly substituted by water molecules. This means that the concentration of one proton donator decreases while the concentration of the other,  $H_3O^+$ , is still low. As a result,  $k_1$  decreases. At higher water contents, the increase in the concentration of the better proton donator  $H_3O^+$  leads to an increase in  $k_1$ , as observed for [DEMA][TfO] and [1-EIm][TfO].
- (ii) A substitution of [2-SEMA]<sup>+</sup> cations by water molecules may also decrease the number of active sites for the adsorption of oxygen molecules: Whereas the bulky [2-SEMA]<sup>+</sup> and [TfO]<sup>-</sup> ions near the Pt surface may probably leave enough space for the adsorption of the much smaller oxygen molecules, water molecules compete with oxygen for adsorption at active sites. A reduced number of active sites match the decrease in the—dominating—pre-exponential factor.
- (iii) As is mentioned above, there are several hints that the water content in the double layer formed by [2-SEMA][TfO]/water mixtures may be higher than that of the bulk electrolyte and even higher than [DEMA][TfO] and [1-EIm][TfO]. If the water content would be high enough, proton transport to the adsorbed oxygen molecules could proceed via a fast co-operative rather than a vehicular mechanism and thus enable the fast supply of protons. It should be noted that, independently of the transport mechanism, the proton donators [2-SEMA]<sup>+</sup> and H<sub>3</sub>O<sup>+</sup> need not be located directly on the Pt surface, which would be unfavorable due to electrostatic repulsion. Rather, they must be close to either bridging O<sub>2</sub> or end-on chemisorbed O<sub>2</sub> molecules, *i.e.*, two or three bonding lengths away from the Pt surface. A fast proton supply supported by water molecules may also explain the pronounced increase in water contents higher than 30 mol%.
- (iv) The activation entropy is affected by the structure and chemical environment of the educts and the activated complex. However, because the surface coverages of PIL ions, oxygen (intermediates), water

and H<sub>3</sub>O<sup>+</sup>, as well as the structure and composition of the inner layers of the double layer are unknown, assumptions regarding the molecular structure and entropy of the different reacting states of the r.d.s. would be fairly speculative. In any case, increasing the bulk water content should affect the activation entropy, as it leads to a higher coverage of H<sub>2</sub>O molecules and greater degree of hydration of the adsorbed species.

A combination of the effects (i)–(iv) would well explain the V-shaped dependence of  $k_1$  on the water content. The above-mentioned correlation of the ORR current density and  $k_1$  to the low frequency pseudocapacitance  $C_2$  (see Figure S6 in the Supporting Information) is especially interesting, as  $C_2$  refers to slow surface processes and thus reflects changes in the adsorbate structure and activation entropy.

# Charge transfer coefficient

Apart from the rate constant  $k_1$ , the cathodic charge transfer coefficient  $\alpha_1$  is a second important parameter that determines the kinetics of the rate-determining step and so the overall ORR kinetics. The higher  $\alpha_1$  is, the more quickly the r.d.s. proceeds. Because n is equal to 1 and the first electron transfer step is rate-determining,  $\alpha_1$  might also be referred to as symmetry factor  $\beta_1$ .<sup>53</sup> Figure 9 shows  $\alpha_1$  as a function of the water content (Figure 9a, T = 70 °C) and temperature (Figure 9b,  $x_{H2O} = 21-23$  mol%). Most of the charge transfer coefficients are within a range of 0.3–0.5, *i.e.*, somewhat lower than  $\alpha_1 \approx 0.5$ , as obtained for diluted aqueous acids. A deviation of the charge transfer from 0.5 is usually explained by an asymmetrical energy barrier of the electron transfer reaction (ETR), which is considered e.g., in the asymmetric Marcus–Hush (AMH) and Matyushov models.<sup>54-56</sup> The stronger the bond between the catalyst and redox partners; the more adiabatic the electron transfer, the more asymmetrical the energy barriers and the larger the deviation from 0.5. However, the aforementioned theories were developed for redox couples of solvated ions and not for adsorbed oxygen molecules, atoms or ions. Moreover, the structure and surroundings of the activated complex, including water,  $H_3O^+$  and the respective PIL ions, is unknown. The same is true for the course of the electric potential in the double layer and the impact of the local electric field on the activated complex.

For these reasons, no simple explanation or quantitative analysis can be given for the  $\alpha_1$  values obtained here.

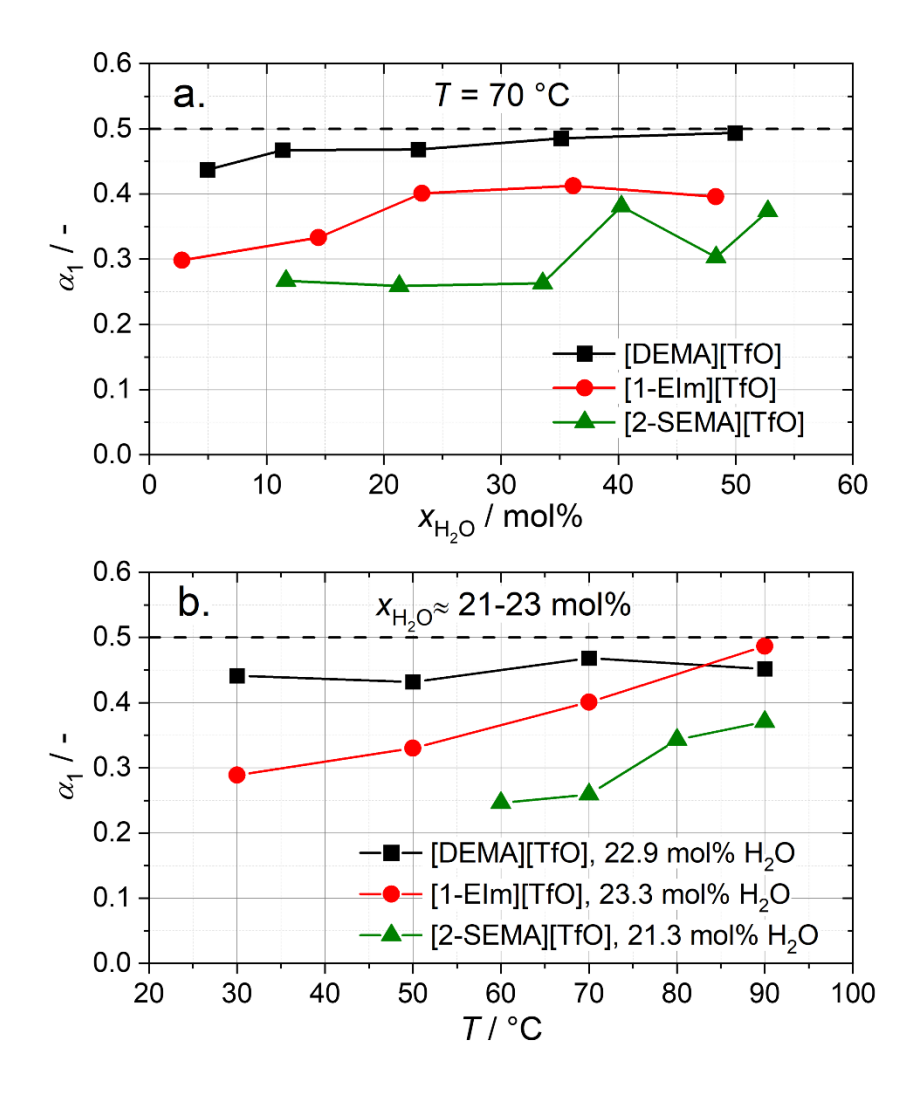


Figure 9. Charge transfer coefficient  $\alpha_1$  of the r.d.s. of ORR; comparison of [DEMA][TfO], [1-EIm][TfO] and [2-SEMA][TfO]: a.  $\alpha_1$  vs. water content for the example of T = 70 °C; b.  $\alpha_1$  vs. temperature for the example of  $x_{H2O} \approx 21-23$  mol%.

It should be noted that the charge transfer coefficients calculated from the Tafel slopes of the IR-corrected U/I curves, obtained by HMRDE experiments at 90 °C and water contents of 17–43 mol%, are in the range of 0.47–0.54 and tend to increase with the water concentration. These values are substantially higher than the  $\alpha_1$  value of 0.37 at 90 °C and 21 mol% H<sub>2</sub>O, as shown in Figure 9a. This is not a contradiction

though, because the  $\alpha$  values obtained from our simulations are intrinsic values but the calculated Tafel slopes and so the corresponding charge transfer coefficients are apparent values, according to Gottesfeld's equation:<sup>57</sup>

$$\frac{d(logj)}{d(U_0 - U)} = \frac{1}{b_{ann}} = \frac{1}{b_{int}} + \left(\frac{1}{1 - \theta_{ox}} \frac{d\theta_{ox}}{dU}\right)$$

The term in parentheses represents the change in the surface coverage of the adsorbed oxygen species with the electrode potential.  $\theta_{ox}$  decreases with decreasing potential (increasing overpotential) and reaches a value close to zero in the potential range of the limiting current density. Therefore,  $b_{app}$  is always smaller than  $b_{int}$  and equal to  $b_{int}$  in the limiting current range. The inverse also holds true, because  $b = -2.3 \text{RT}/\alpha \text{F}$ , and  $\alpha_{app}$  is always higher than  $\alpha_{int}$ . This corresponds precisely to the higher apparent values of the charge transfer coefficient obtained from the Tafel slopes.

As can be seen from Figure 9, there is a tendency for  $\alpha_1$  to increase with the temperature and water content up to the value of 0.5, but to decrease with the increasing acidity of the PIL. This seems logical, as the surrounding environment of the activated complex during the charge transfer, especially the innermost layer adjacent to the Pt surface, changes in a way that it will become similar to an environment typical for aqueous solutions: the increase in water content and temperature leads to a fewer ions and higher water adsorption and to a lower stiffness in the innermost layer.<sup>15, 29</sup> With decreasing acidity of the PIL cation,  $H_3O^+$  increasingly dominates as a proton donator, which is also the case in aqueous solutions.

## **CONCLUSIONS**

Proton-conducting ionic liquids (PILs) are promising candidates as electrolytes for mid-temperature PEM fuel cells operating at temperatures of 100-120 °C. The improvement of the ORR kinetics at the Pt/PIL interface in the fuel cell cathode is still an issue, however. Because water is produced at the cathode, the PILs always contain certain amounts of it, depending on the operating conditions. Therefore, mixtures of PILs and water in the range of  $\approx 3-50$  mol% were used as electrolytes. One of the important material

properties of the PIL, which affects the ORR kinetics, is the acidity of the PIL cation. A high acidity should not only improve the proton-donating ability of the cation itself though: In equilibrium with water, acidic cations generate a large concentration of the effective proton donator  $H_3O^+$ . However, former results suggest the strongly acidic [2-SEMA]<sup>+</sup> cation (p $K_a$  = 0.94) to be a poor proton donator in  $H_{UPD}$ . Therefore, one important aspect of this work was to determine whether or not [2-SEMA]<sup>+</sup> cations are effective proton donators in ORR. The main goal of this was to compare the ORR kinetics in the Pt/[2-SEMA][TfO] interface with those of two other ionic liquids with a much lower acidity of the cation, *i.e.*, [DEMA][TfO] (p $K_a$  = 10.55) and [1-EIm][TfO] (p $K_a$  = 7.30). The main conclusions of this work can be summarized as follows:

- Both the acidity and water content have a large influence on the ORR kinetics on Pt. The effects cannot be completely separated, because the concentration of the proton donator H<sub>3</sub>O<sup>+</sup> that is generated by the protolysis equilibrium of the PIL cation and water depends on the water content. Only the acidic [2-SEMA][TfO] provides reasonable ORR current densities under application-relevant potentials > 0.4 V. In contrast, PILs with low acidities such as [DEMA][TfO] and [1-EIm][TfO] appear to be unsuitable as (sole) electrolytes in PEFCs for intermediate operation temperatures.
- However, the ORR limiting current of the low-acidic PILs [DEMA][TfO] and [1-EIm][TfO] is about one order of magnitude higher than that of [2-SEMA][TfO], which is due to a correspondingly higher  $D_{O_2} c_{O_2}$  product. In contrast, the low diffusion coefficient and concentration of oxygen makes [2-SEMA][TfO] unsuitable for application at low cathode potentials and high current densities, respectively. This suggests that a mixture of PILs with a high proton donating ability in the relevant range of water content and those with superior bulk properties, *i.e.*, combining the favorable properties of PILs, would be a suitable approach.
- According to the protolysis equilibria, the H<sub>3</sub>O<sup>+</sup> concentration increases with the water content. It is therefore logical that [DEMA][TfO] and [1-EIm][TfO] show an increase in the ORR performance with increasing water and H<sub>3</sub>O<sup>+</sup> concentrations. In contrast, [2-SEMA][TfO] exhibits a minimum of the current density and the rate constant at a medium water content of about 30 mol%. This means that at low water contents, the ORR rate increases rather than decreases. Clearly, the [2-SEMA]<sup>+</sup> cation is a

good proton donator in ORR, contrary to the former results obtained for the  $H_{UPD}$  reaction. This apparent contradiction can be explained by a poisoning or blocking effect through the conjugated base N-methyltaurine in the  $H_{UPD}$  range, but must be confirmed by future experiments, including measurements of the PZC and the adsorbate structure.

- The minimum ORR rate can only partially be explained by the much higher acidity and proton-donating ability of the [2-SEMA]<sup>+</sup> cation compared to [DEMA]<sup>+</sup> and [1-EIm]<sup>+</sup>. This effect appears to be governed by the pre-exponential factor of the rate constant and is tentatively explained in terms of the favorable and disadvantageous effects of water, *i.e.*, the generation of H<sub>3</sub>O<sup>+</sup>, faster proton transport, the substitution of [2-SEMA]<sup>+</sup> cations and the blocking of active sites. The lowest performance at about 30 mol% H<sub>2</sub>O is unfavorable, because a water content of 20-30 mol% is assumed to be typical for PEFC operation at temperatures of about 120 °C. For future work, it is important to enhance the ORR rate, especially under these conditions.
- The charge transfer coefficient of the r.d.s.,  $\alpha_1$ , is typically in the range from 0.3–0.5. It decreases with increasing acidity of the PIL cation and tends to increase with the temperature and water content. Although no quantitative analysis, *e.g.*, in terms of asymmetrical energy barriers of the ETR can be given here, and there is a clear tendency of  $\alpha_1$  to approach a value of 0.5, and if the experimental conditions favor a structure of the Pt/PIL interface, similar to that in aqueous solutions.
- Apart from the acidity of the cation, other material and molecular properties of the PIL, such as steric effects, the hygroscopicity and ability to form hydrogen bonds, may influence the ORR kinetic parameters as well. Because of the interdependencies of some properties, the correlation of parameters like  $k_1$  and  $\alpha_1$  with only a single property of the actual PIL must be undertaken with care. Therefore, future work should aim to unravel these effects as much as possible.

The correlation of the ORR rate constant  $k_1$  and the pseudo-double layer capacitance  $C_2$  is a very interesting result that deserves further investigations. In a sense, the pseudo-double layer capacitance can be regarded as a link between the ORR kinetics and the structure of the innermost/adsorbate layer. Besides electrochemical methods, future experiments should also comprise sensitive surface techniques, such as

AFM and IR spectroscopy, as well as molecular dynamics of the Pt/PIL interface. This would contribute to a better understanding of the ORR kinetics as a function of the structure and properties of the double layer, especially the innermost layer, as well as the adsorbed species and activated complex.

#### SUPPORTING INFORMATION

(a) Total number of transferred electrons for the ORR on a Pt micro electrode in [1-EIm][TfO]/H<sub>2</sub>O (Fig. S1): (b) Reaction order of ORR with respect to the  $O_2$  concentration for [2-SEMA][TfO]/H<sub>2</sub>O, [DEMA][TfO]/H<sub>2</sub>O and [1-EIm][TfO]/H<sub>2</sub>O (Fig. S2); (c) Influence of the type of proton donator on the simulation of CVs of ORR on Pt (Fig. S3); (d) Double logarithmic plots of  $D_{O_2}$  vs. water content for [DEMA][TfO], [1-EIm][TfO] and [2-SEMA][TfO] (Fig. S4); (e) Double logarithmic plots of  $C_{O_2}$  vs. water content for [DEMA][TfO], [1-EIm][TfO] and [2-SEMA][TfO] (Fig. S5); (f) [2-SEMA][TfO]/H<sub>2</sub>O: Current density, rate constant and pseudo double layer capacitance vs. water content (Fig. S6); (g) Table of  $C_{H3O+}$  values for [DEMA][TfO], [1-EIm][TfO] and [2-SEMA][TfO] (see Table S1); (h) Table of  $C_{H2O}$  values for [DEMA][TfO], [1-EIm][TfO] and [2-SEMA][TfO] (see Table S2).

## **ACKNOWLEDGEMENTS**

We gratefully acknowledge the preparation of the micro- and macro-electrodes by A. Schwaitzer (ZEA-1). We are grateful to K. Klafki for her assistance in Karl-Fischer titration and to L. Bürgers for carrying out the water-uptake experiment. We are also obliged to C. Wood for proofreading the manuscript.

#### REFERENCES

- (1) Zhang, J.; Tang, Y.; Song, C.; Zhang, J., Polybenzimidazole-Membrane-Based PEM Fuel Cell in the Temperature Range of 120–200 °C. *J. Power Sources* **2007**, *172*, 163-171.
- (2) Scharifker, B. R.; Zelenay, P.; Bockris, J. O. M., The Kinetics of Oxygen Reduction in Molten Phosphoric Acid at High Temperatures. *J. Electrochem. Soc.* **1987**, *134*, 2714-2725.

- (3) Mitsushima, S.; Shinohara, Y.; Matsuzawa, K.; Ota, K.-i., Mass Transportation in Diethylmethylammonium Trifluoromethanesulfonate for Fuel Cell Applications. *Electrochim. Acta* **2010**, *55*, 6639-6644.
- (4) Nakamoto, H.; Watanabe, M., Bronsted Acid-Base Ionic Liquids for Fuel Cell Electrolytes. *Chem. Commun. (Cambridge, U. K.)* **2007**, 2539-2541.
- (5) Wippermann, K.; Wackerl, J.; Lehnert, W.; Huber, B.; Korte, C., 2-Sulfoethylammonium Trifluoromethanesulfonate as an Ionic Liquid for High Temperature PEM Fuel Cells. *J. Electrochem. Soc.* **2016**, *163*, F25-F37.
- (6) Wippermann, K.; Suo, Y.; Korte, C., Suitability of the Hanging Meniscus RDE for the Electrochemical Investigation of Ionic Liquids. *J. Electrochem. Soc.* **2020**, *167*, 046511.
- (7) Khan, A.; Gunawan, C. A.; Zhao, C., Oxygen Reduction Reaction in Ionic Liquids: Fundamentals and Applications in Energy and Sensors. *ACS Sustainable Chem. Eng.* **2017**, *5*, 3698-3715.
- (8) Zhang, Y.; Pozo-Gonzalo, C., Variations and Applications of the Oxygen Reduction Reaction in Ionic Liquids. *Chem. Commun.* (*Cambridge, U. K.*) **2018**, *54*, 3800-3810.
- (9) Gui, A. L.; Endres, F.; Wittstock, G., Influence of Chemical Structure and Temperature on Oxygen Reduction Reaction and Transport in Ionic Liquids. *Z. Phys. Chem. (Muenchen, Ger.)* **2017**, *231*, 1077-1092.
- (10) Belieres, J.-P.; Angell, C. A., Protic Ionic Liquids: Preparation, Characterization, and Proton Free Energy Level Representation. *J. Phys. Chem. B* **2007**, *111*, 4926-4937.
- (11) Miran, M. S.; Yasuda, T.; Susan, M. A. B. H.; Dokko, K.; Watanabe, M., Electrochemical Properties of Protic Ionic Liquids: Correlation between Open Circuit Potential for H2/O2 Cells under Non-Humidified Conditions and Δpka. *RSC Adv.* **2013**, *3*, 4141-4144.
- (12) Miran, M. S.; Yasuda, T.; Susan, M. A. B. H.; Dokko, K.; Watanabe, M., (Keynote) Protic Ionic Liquids Based on a Super-Strong Acid: Bulk and Electrochemical Properties. *ECS Trans.* **2013**, *50*, 285-291.
- (13) Trummal, A.; Lipping, L.; Kaljurand, I.; Koppel, I. A.; Leito, I., Acidity of Strong Acids in Water and Dimethyl Sulfoxide. *J. Phys. Chem. A* **2016**, *120*, 3663-3669.
- (14) Wippermann, K.; Giffin, J.; Korte, C., In Situ Determination of the Water Content of Ionic Liquids. *J. Electrochem. Soc.* **2018**, *165*, H263-H270.
- Wippermann, K.; Giffin, J.; Kuhri, S.; Lehnert, W.; Korte, C., The Influence of Water Content in a Proton-Conducting Ionic Liquid on the Double Layer Properties of the Pt/Pil Interface. *Phys. Chem. Chem. Phys.* **2017**, *19*, 24706-24723.
- (16) Ejigu, A.; Walsh, D. A., The Role of Adsorbed Ions During Electrocatalysis in Ionic Liquids. *J. Phys. Chem. C* **2014**, *118*, 7414-7422.
- (17) Munakata, H.; Tashita, T.; Haibara, M.; Kanamura, K., Synthesis of New Protic Ionic Liquids for Fuel Cells on the Basis of in-Situ Ft-Ir Measurements. *ECS Trans.* **2010**, *33*, 463-469.
- (18) Kiatkittikul, P.; Yamaguchi, J.; Taniki, R.; Matsumoto, K.; Nohira, T.; Hagiwara, R., Influence of Cationic Structures on Oxygen Reduction Reaction at Pt Electrode in Fluorohydrogenate Ionic Liquids. *J. Power Sources* **2014**, *266*, 193-197.
- (19) Zhang, G.-R.; Munoz, M.; Etzold, B. J. M., Boosting Performance of Low Temperature Fuel Cell Catalysts by Subtle Ionic Liquid Modification. *ACS Appl. Mater. Interfaces* **2015**, *7*, 3562-70.
- (20) Snyder, J.; Fujita, T.; Chen, M. W.; Erlebacher, J., Oxygen Reduction in Nanoporous Metal–Ionic Liquid Composite Electrocatalysts. *Nat. Mater.* **2010**, *9*, 904-907.
- (21) Zhang, G.-R.; Munoz, M.; Etzold, B. J. M., Accelerating Oxygen-Reduction Catalysts through Preventing Poisoning with Non-Reactive Species by Using Hydrophobic Ionic Liquids. *Angew. Chem. Int. Ed.* **2016**, *55*, 2257-2261.
- (22) Huang, K.; Song, T.; Morales-Collazo, O.; Jia, H.; Brennecke, J. F., Enhancing Pt/C Catalysts for the Oxygen Reduction Reaction with Protic Ionic Liquids: The Effect of Anion Structure. *J. Electrochem. Soc.* **2017**, *164*, F1448-F1459.
- (23) Kudo, K.; Mitsushima, S.; Kamiya, N.; Ota, K.-i., Ionic Conductivity and Oxygen Reduction Reaction on Pt in Proton Conductive Room Temperature Molten Salts for 2-Alkylimidazolium and Bronsted-Acid Added Systems. *Electrochemistry (Tokyo, Jpn.)* **2005**, *73*, 668-674.

- Goodwin, S. E.; Smith, D. E.; Gibson, J. S.; Jones, R. G.; Walsh, D. A., Electroanalysis of Neutral Precursors in Protic Ionic Liquids and Synthesis of High-Ionicity Ionic Liquids. *Langmuir* **2017**, *33*, 8436-8446.
- (25) SciFinder, value taken from substance search with substance identifier ,616-39-7', predicted value calculated using Advanced Chemistry Development (ACD/Labs) Software V11.02 **2017**.
- (26) Stoimenovski, J.; Izgorodina, E. I.; MacFarlane, D. R., Ionicity and Proton Transfer in Protic Ionic Liquids. *Phys. Chem. Chem. Phys.* **2010**, *12*, 10341-10347.
- (27) Friedl, J.; Markovits, I. I. E.; Herpich, M.; Feng, G.; Kornyshev, A. A.; Stimming, U., Interface between an Au(111) Surface and an Ionic Liquid: The Influence of Water on the Double-Layer Capacitance. *ChemElectroChem* **2017**, *4*, 216-220.
- (28) Feng, G.; Jiang, X.; Qiao, R.; Kornyshev, A. A., Water in Ionic Liquids at Electrified Interfaces: The Anatomy of Electrosorption. *ACS Nano* **2014**, *8*, 11685-11694.
- (29) Zhong, Y.; Yan, J.; Li, M.; Chen, L.; Mao, B., The Electric Double Layer in an Ionic Liquid Incorporated with Water Molecules: Atomic Force Microscopy Force Curve Study. *ChemElectroChem* **2016**, *3*, 2221-2226.
- (30) Motobayashi, K.; Osawa, M., Potential-Dependent Condensation of Water at the Interface between Ionic Liquid [Bmim][Tfsa] and an Au Electrode. *Electrochem. Commun.* **2016**, *65*, 14-17.
- Vainikka, T.; Figueiredo, M. C.; Kontturi, K.; Murtomaki, L., Studies of Oxygen Reduction in 1-Butyl-1-Methylpyrrolidinium Bis(Trifluoromethylsulfonyl)Imide by Microdisk Voltammetry. *Electrochim. Acta* **2015**, *156*, 60-69.
- (32) Lenarcik, B.; Ojczenasz, P., The Influence of the Size and Position of the Alkyl Groups in Alkylimidazole Molecules on Their Acid-Base Properties. *J. Heterocyclic Chem.* **2002**, *39*, 287-290.
- (33) SciFinder, value taken from substance search with substance identifier ,107-68-6', predicted value calculated using Advanced Chemistry Development (ACD/Labs) Software V11.02 **2017**.
- (34) Lin, J.; Wang, L.; Zinkevich, T.; Indris, S.; Suo, Y.; Korte, C., Influence of Residual Water and Cation Acidity on the Ionic Transport Mechanism in Proton-Conducting Ionic Liquids. *Phys. Chem. Chem. Phys.* **2020**, 22, 1145-1153.
- (35) Shoup, D.; Szabo, A., Chronoamperometric Current at Finite Disk Electrodes. *J. Electroanal. Chem. Interfacial Electrochem.* **1982**, *140*, 237-45.
- (36) Katsounaros, I.; Schneider, W. B.; Meier, J. C.; Benedikt, U.; Biedermann, P. U.; Auer, A. A.; Mayrhofer, K. J. J., Hydrogen Peroxide Electrochemistry on Platinum: Towards Understanding the Oxygen Reduction Reaction Mechanism. *Phys. Chem. Chem. Phys.* **2012**, *14*, 7384-7391.
- (37) Wang, H.; Capuano, G. A., Behavior of Raipore Radiation-Grafted Polymer Membranes in H 2 / O 2 Fuel Cells. *J. Electrochem. Soc.* **1998**, *145*, 780-784.
- (38) Mack, F.; Aniol, K.; Ellwein, C.; Kerres, J.; Zeis, R., Novel Phosphoric Acid-Doped PBI-Blends as Membranes for High-Temperature PEM Fuel Cells. *J. Mater. Chem. A* **2015**, *3*, 10864-10874.
- (39) Walsh, D. A.; Ejigu, A.; Smith, J.; Licence, P., Kinetics and Mechanism of Oxygen Reduction in a Protic Ionic Liquid. *Phys. Chem. Chem. Phys.* **2013**, *15*, 7548-54.
- (40) Khan, A.; Lu, X.; Aldous, L.; Zhao, C., Oxygen Reduction Reaction in Room Temperature Protic Ionic Liquids. *J. Phys. Chem. C* **2013**, *117*, 18334-18342.
- (41) Markovic, N. M.; Adzic, R. R.; Cahan, B. D.; Yeager, E. B., Structural Effects in Electrocatalysis: Oxygen Reduction on Platinum Low Index Single-Crystal Surfaces in Perchloric Acid Solutions. *J. Electroanal. Chem.* **1994**, *377*, 249-59.
- (42) Damjanovic, A.; Sepa, D. B.; Vojnovic, M. V., New Evidence Supports the Proposed Mechanism for Dioxygen Reduction at Oxide Free Platinum Electrodes. *Electrochim. Acta* **1979**, *24*, 887-9.
- (43) Liu, Z.; Wainright, J. S.; Litt, M. H.; Savinell, R. F., Study of the Oxygen Reduction Reaction (ORR) at Pt Interfaced with Phosphoric Acid Doped Polybenzimidazole at Elevated Temperature and Low Relative Humidity. *Electrochim. Acta* **2006**, *51*, 3914-3923.

- (44) Switzer, E. E.; Zeller, R.; Chen, Q.; Sieradzki, K.; Buttry, D. A.; Friesen, C., Oxygen Reduction Reaction in Ionic Liquids: The Addition of Protic Species. *J. Phys. Chem. C* **2013**, *117*, 8683-8690.
- (45) Drueschler, M.; Huber, B.; Passerini, S.; Roling, B., Hysteresis Effects in the Potential-Dependent Double Layer Capacitance of Room Temperature Ionic Liquids at a Polycrystalline Platinum Interface. *J. Phys. Chem. C* **2010**, *114*, 3614-3617.
- (46) Santos, M. C.; Miwa, D. W.; Machado, S. A. S., Study of Anion Adsorption on Polycrystalline Pt by Electrochemical Quartz Crystal Microbalance. *Electrochem. Commun.* **2000**, *2*, 692-696.
- (47) Ojha, K.; Arulmozhi, N.; Aranzales, D.; Koper, M. T. M., Double Layer at the Pt(111)–Aqueous Electrolyte Interface: Potential of Zero Charge and Anomalous Gouy–Chapman Screening. *Angew. Chem. Int. Ed.* **2020**, *59*, 711-715.
- (48) Berná, A.; Feliu, J. M.; Gancs, L.; Mukerjee, S., Voltammetric Characterization of Pt Single Crystal Electrodes with Basal Orientations in Trifluoromethanesulphonic Acid. *Electrochem. Commun.* **2008**, *10*, 1695-1698.
- (49) Goodwin, S. E.; Muhammad, S.; Tuan, L.-P.; Walsh, D. A., The Contrasting Effects of Diethylmethylamine During Reduction of Protons and Oxidation of Formic Acid in Diethylmethylammonium-Based Protic Ionic Liquids. *J. Electroanal. Chem.* **2018**, *819*, 187-192.
- (50) Conway, B. E.; Dhar, H. P., Compensation Effects in the Thermodynamics of Electrochemical Adsorption of Organic Substances. *Colloid Polym. Sci.* **1975**, *253*, 11-21.
- (51) Perez-Benito, J. F.; Mulero-Raichs, M., Enthalpy–Entropy Compensation Effect in Chemical Kinetics and Experimental Errors: A Numerical Simulation Approach. *J. Phys. Chem. A* **2016**, 120, 7598-7609.
- (52) Grgur, B. N.; Markovic, N. M.; Ross, P. N., Temperature-Dependent Oxygen Electrochemistry on Platinum Low-Index Single Crystal Surfaces in Acid Solutions. *Can. J. Chem.* **1997**, *75*, 1465-1471.
- (53) Guidelli, R.; Compton, R. G.; Feliu, J. M.; Gileadi, E.; Lipkowski, J.; Schmickler, W.; Trasatti, S., Defining the Transfer Coefficient in Electrochemistry: An Assessment (Iupac Technical Report). *Pure Appl. Chem.* **2014**, *86*, 245-258.
- (54) Matyushov, D. V., Standard Electrode Potential, Tafel Equation, and the Solvation Thermodynamics. *J. Chem. Phys.* **2009**, *130*, 234704.
- (55) Laborda, E.; Henstridge, M. C.; Batchelor-McAuley, C.; Compton, R. G., Asymmetric Marcus–Hush Theory for Voltammetry. *Chem. Soc. Rev.* **2013**, *42*, 4894-4905.
- (56) Laborda, E.; Henstridge, M. C.; Compton, R. G., Asymmetric Marcus Theory: Application to Electrode Kinetics. *J. Electroanal. Chem.* **2012**, *667*, 48-53.
- (57) Gottesfeld, S., Some Observations on the Oxygen Reduction Reaction (ORR) at Platinum Catalysts Based on Post Year 2000 Reports. *ECS Trans.* **2008**, *6*, 51-67.

## **Figure Captions:**

- Figure 1. Structures of the PILs and  $pK_a$  values of the cations.
- Figure 2. Scheme of possible ORR mechanisms, adapted from Katsounaros et al.<sup>36</sup>
- Figure 3. Cyclic voltammograms (broken lines) and simulated data (full red lines) of ORR on Pt in PIL/water electrolytes as a function of the water content; a comparison of [DEMA][TfO], [1-EIm][TfO] and [2-SEMA][TfO] to the examples of  $T = 90^{\circ}C$  and 35-40 mol% H<sub>2</sub>O.
- Figure 4. CVs (broken lines) and simulated data (full red lines) of ORR on Pt for a. [DEMA][TfO], b. [1-EIm][TfO] and c. [2-SEMA][TfO] at various water contents for the example of T = 70 °C.

Figure 5. Simulated rate constant  $k_1$  of the r.d.s. of the ORR as a function of the water content; a.: comparison of [DEMA][TfO], [1-EIm][TfO] and [2-SEMA][TfO] for the example of T = 90 °C; b.-d.: plots of  $k_1$  vs. the water content for the three PILs at various temperatures; on the right axis, the concentrations of oxygen,  $H_3O^+$  and cations are plotted as well; the polynomial fits (full red lines) only serve as a visual guide.

Figure 6. CVs (broken lines) and simulated data (full red lines) of ORR on Pt for a. [DEMA][TfO], b. [1-EIm][TfO] and c. [2-SEMA][TfO] at various temperatures for the example of a water content of  $\approx$ 21-23 mol%.

Figure 7. Arrhenius plots of  $k_1$ ; a.: comparison of [DEMA][TfO], [1-EIm][TfO] and [2-SEMA][TfO] for the example of  $x_{H2O} \approx 21-23$  mol%; b.-d.: Arrhenius plots of  $k_1$  for the three PILs with various water contents.

Figure 8. Activation energy (a.) and pre-exponential factor (b.) of  $k_1$  derived from the linear fits of the Arrhenius plots shown in Figure 7.

Figure 9. Charge transfer coefficient  $\alpha_1$  of the r.d.s. of ORR; comparison of [DEMA][TfO], [1-EIm][TfO] and [2-SEMA][TfO]: a.  $\alpha_1$  vs. water content for the example of T = 70 °C; b.  $\alpha_1$  vs. temperature for the example of  $x_{H2O} \approx 21-23$  mol%.

Table 1.  $D_{O_2}$  values for [DEMA][TfO], [1-EIm][TfO] and [2-SEMA][TfO] at the experimental conditions of the cyclic voltammograms; data is taken from the fit curves in Figure S1a.

Table 2.  $C_{O_2}$  values for [DEMA][TfO], [1-EIm][TfO] and [2-SEMA][TfO] at the experimental conditions of the cyclic voltammograms; data taken from the fit curves in Figure S1b.

Figure 1

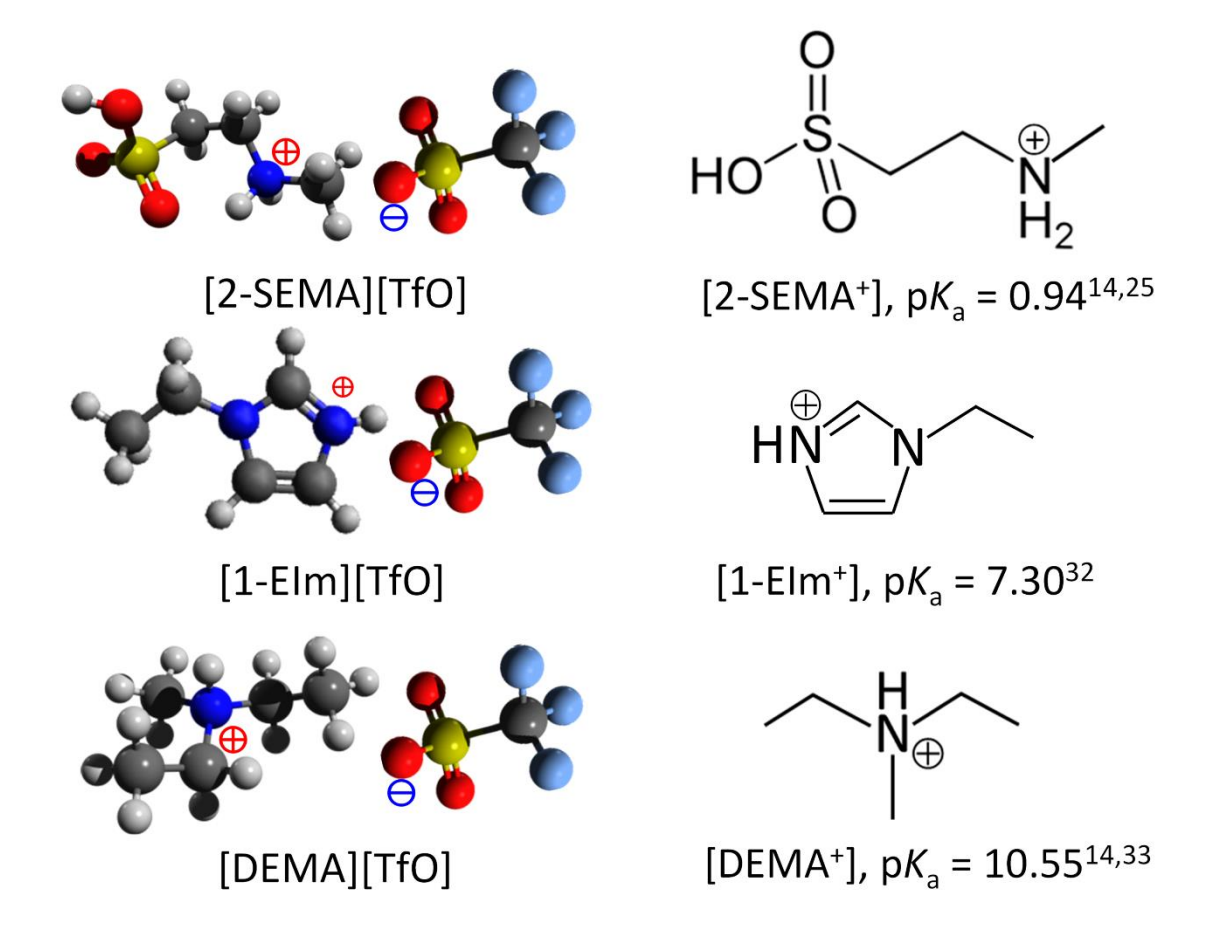


Figure 2

## a. dissociative mechanism $O_{2,PIL} \longrightarrow O_{2,ad} \xrightarrow{+e^-+H^+} HOO_{ad} \xrightarrow{+e^-+H^+} HOOH_{ad} \longrightarrow 2OH_{ad} \longrightarrow 2H_2O_{PIL}$ $O_{2,PIL} \longrightarrow O_{ad} + OH_{ad} \xrightarrow{+e^-+H^+}$ C. associative mechanism

Figure 3

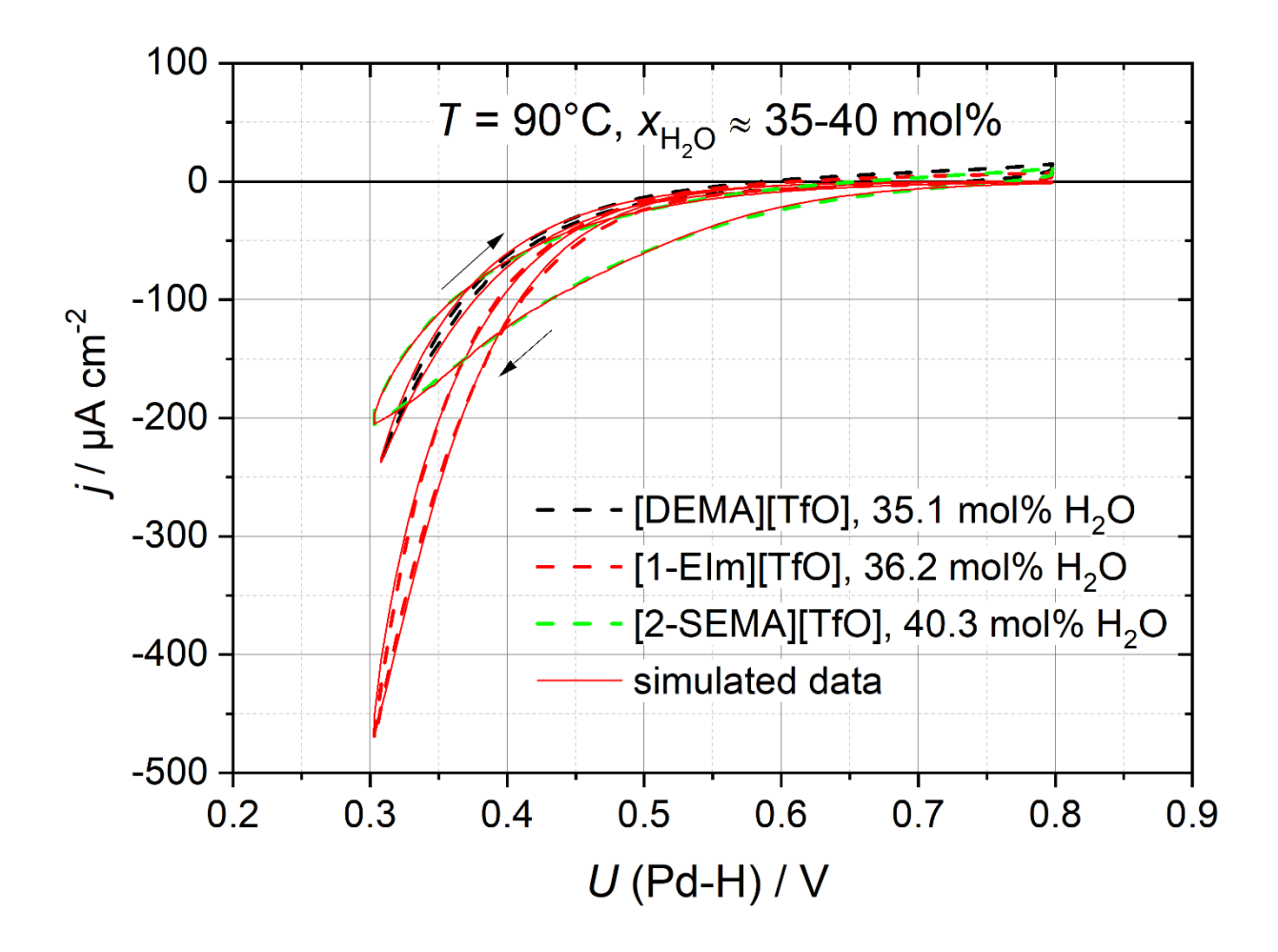


Figure 4 a-c

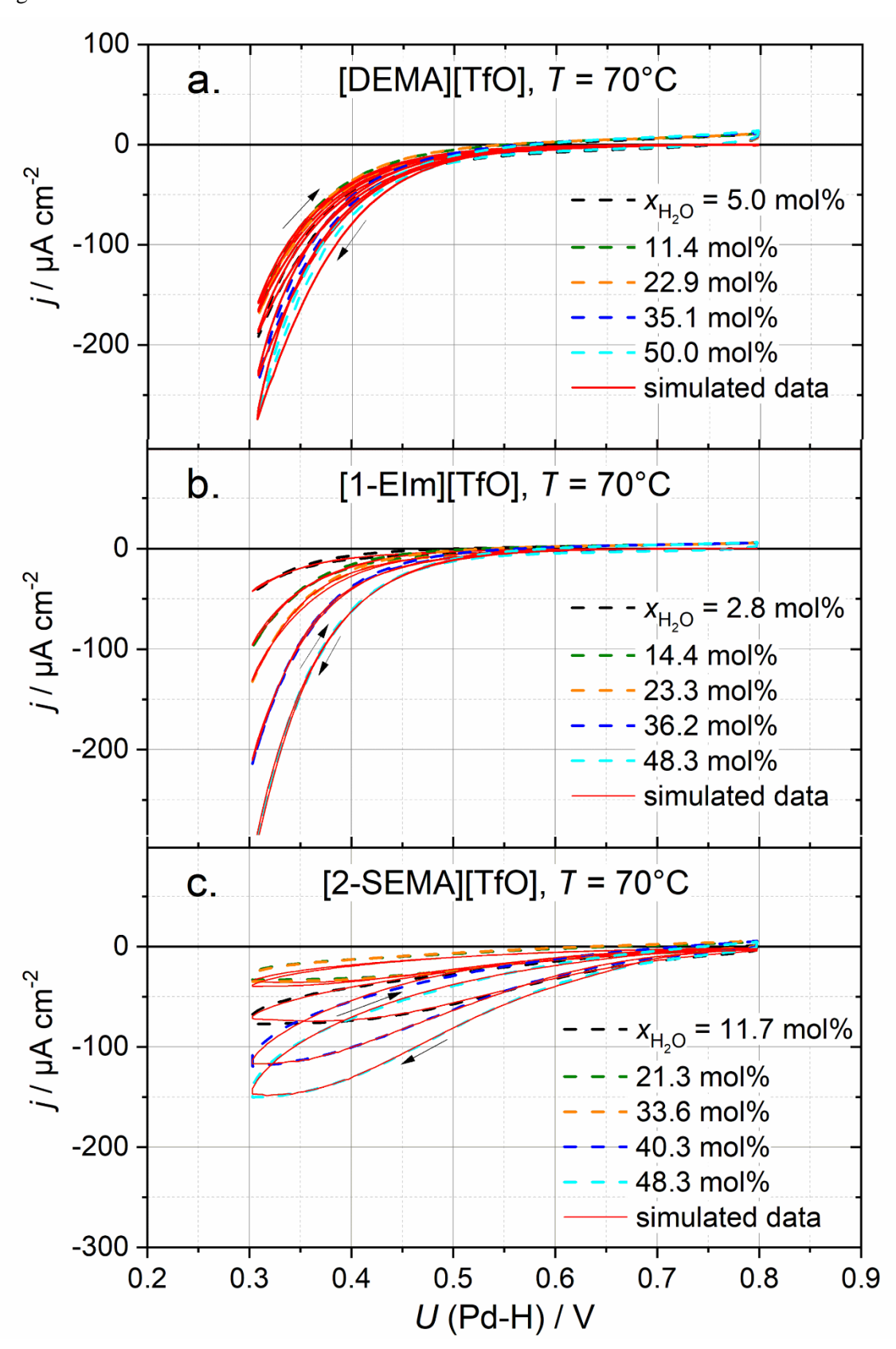
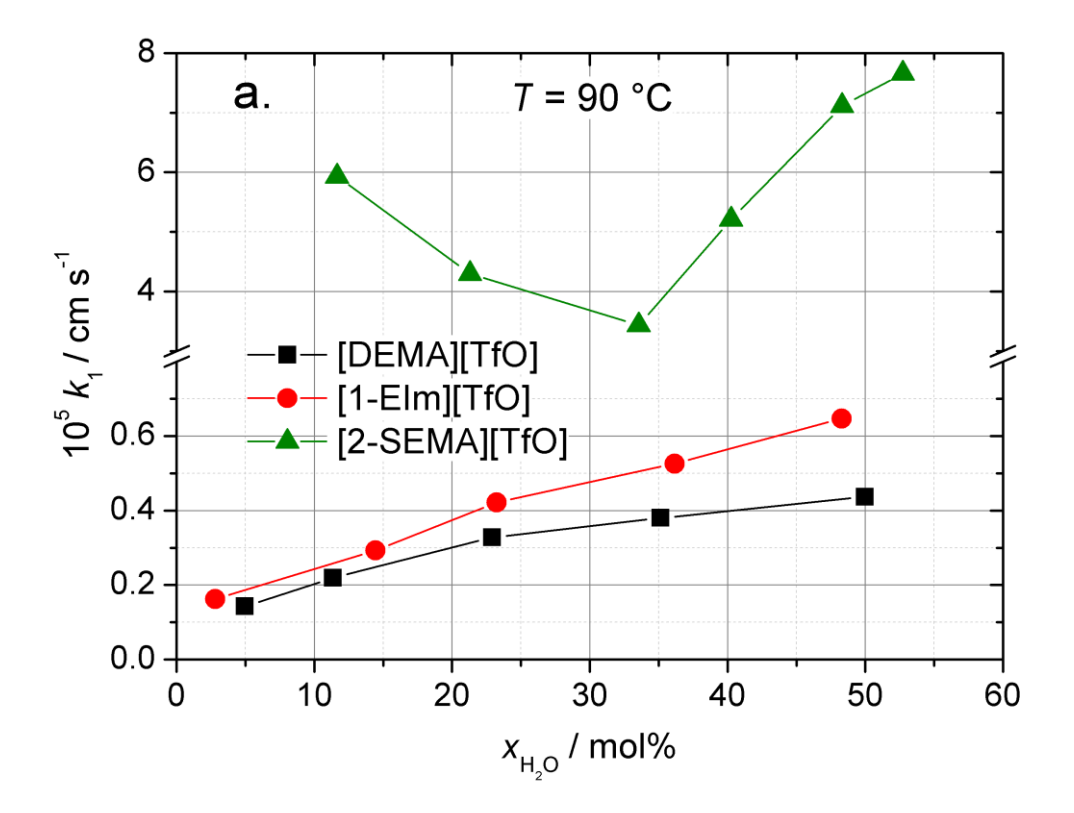
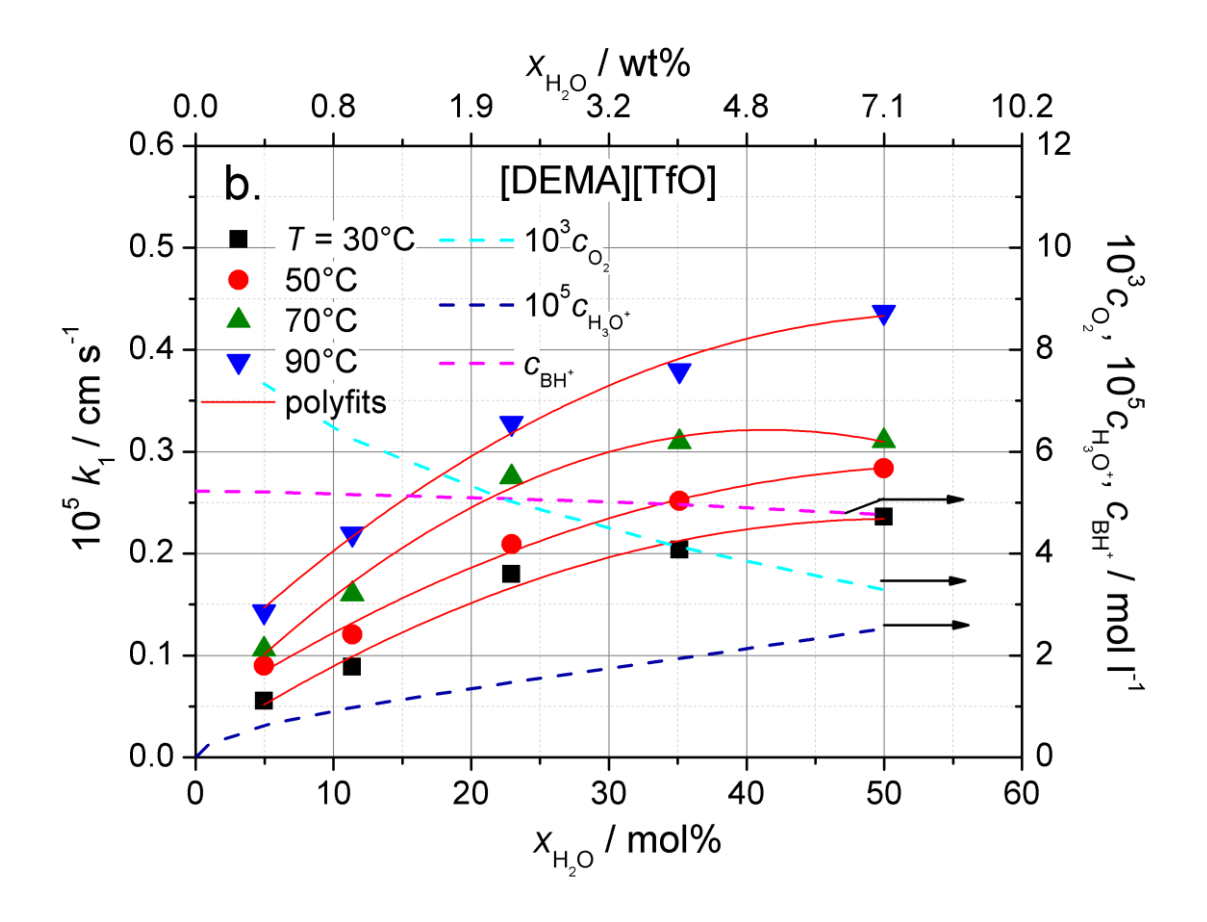


Figure 5





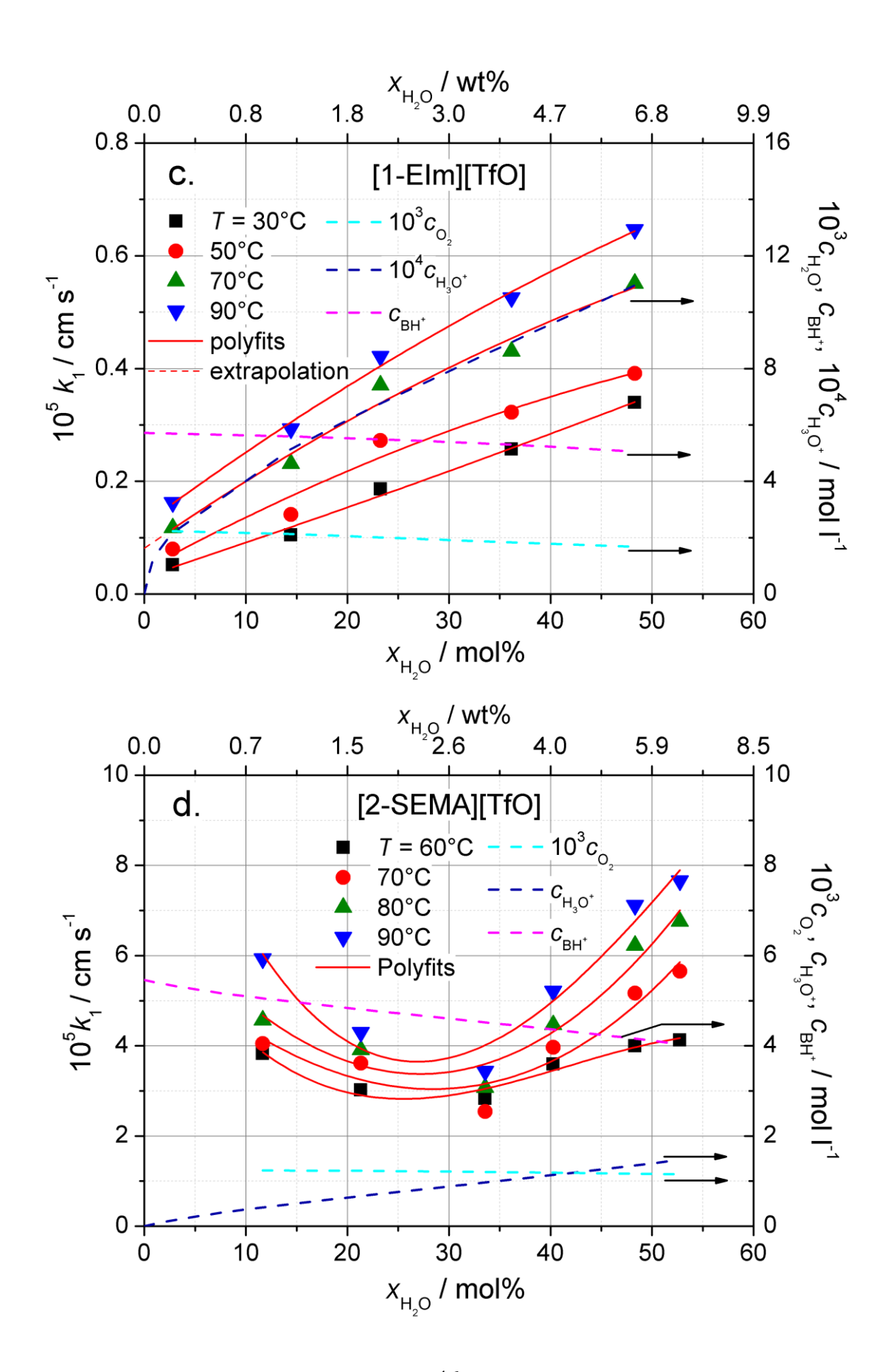


Figure 6

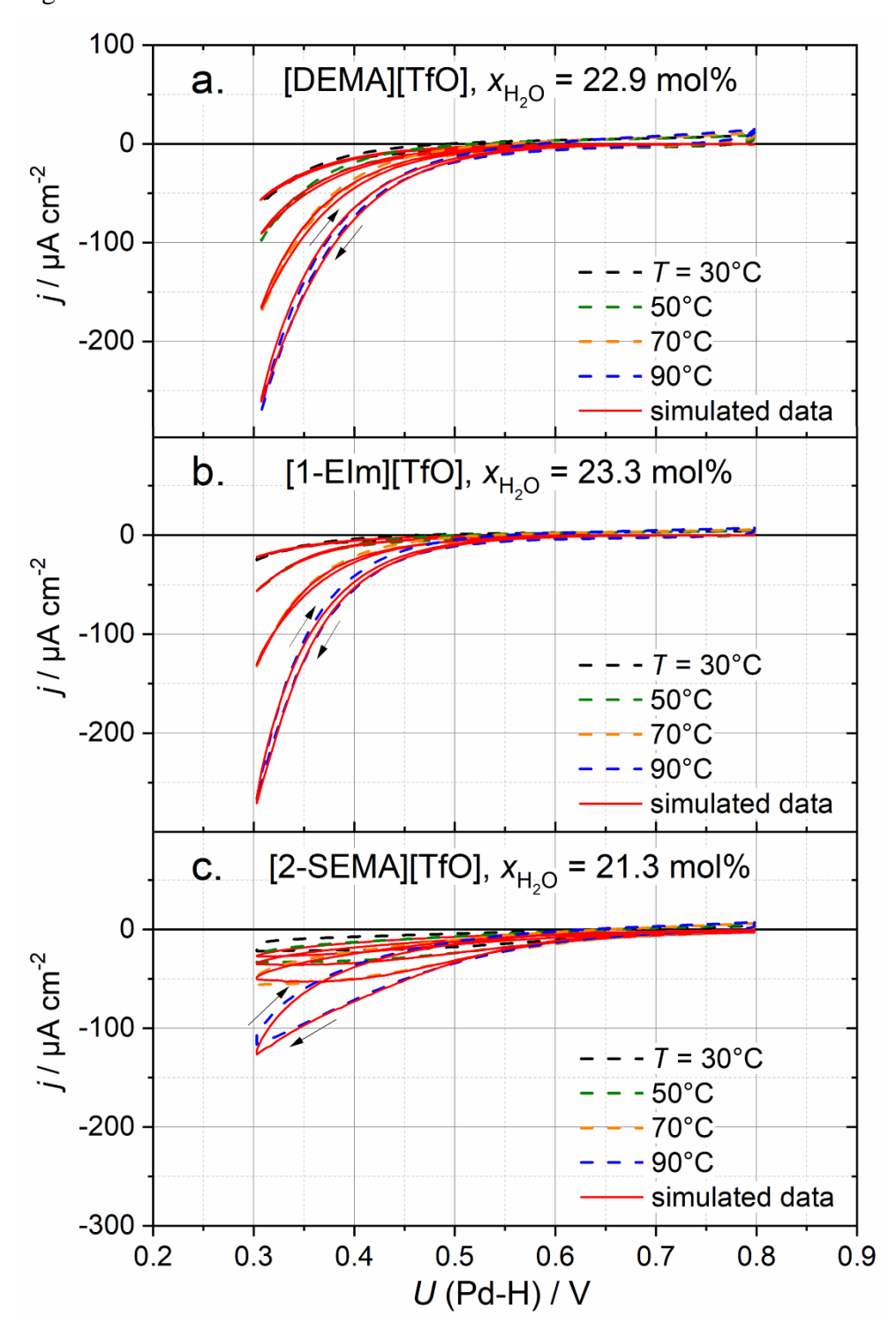
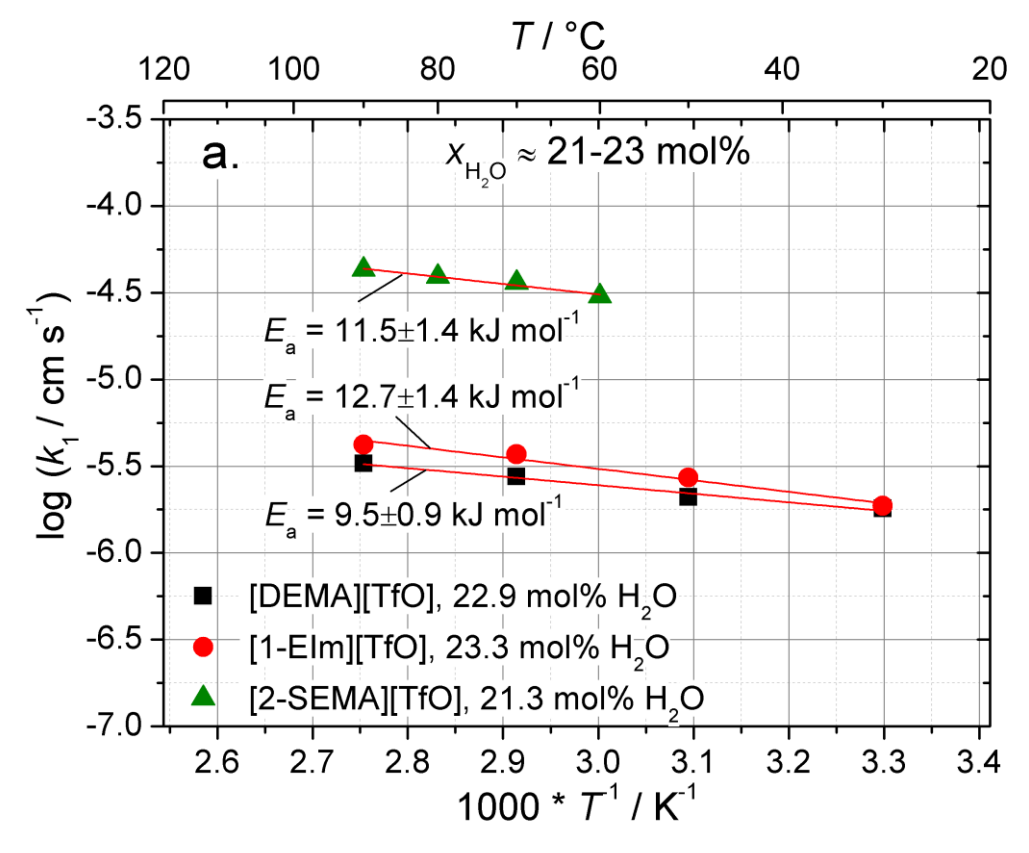
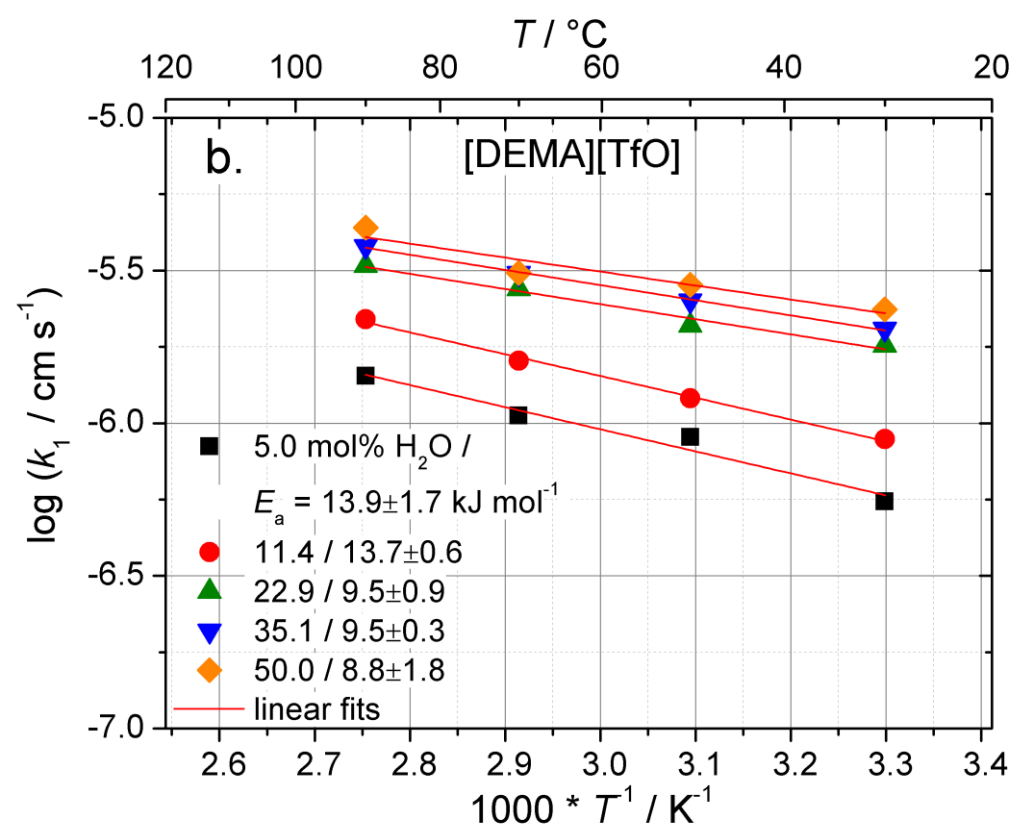
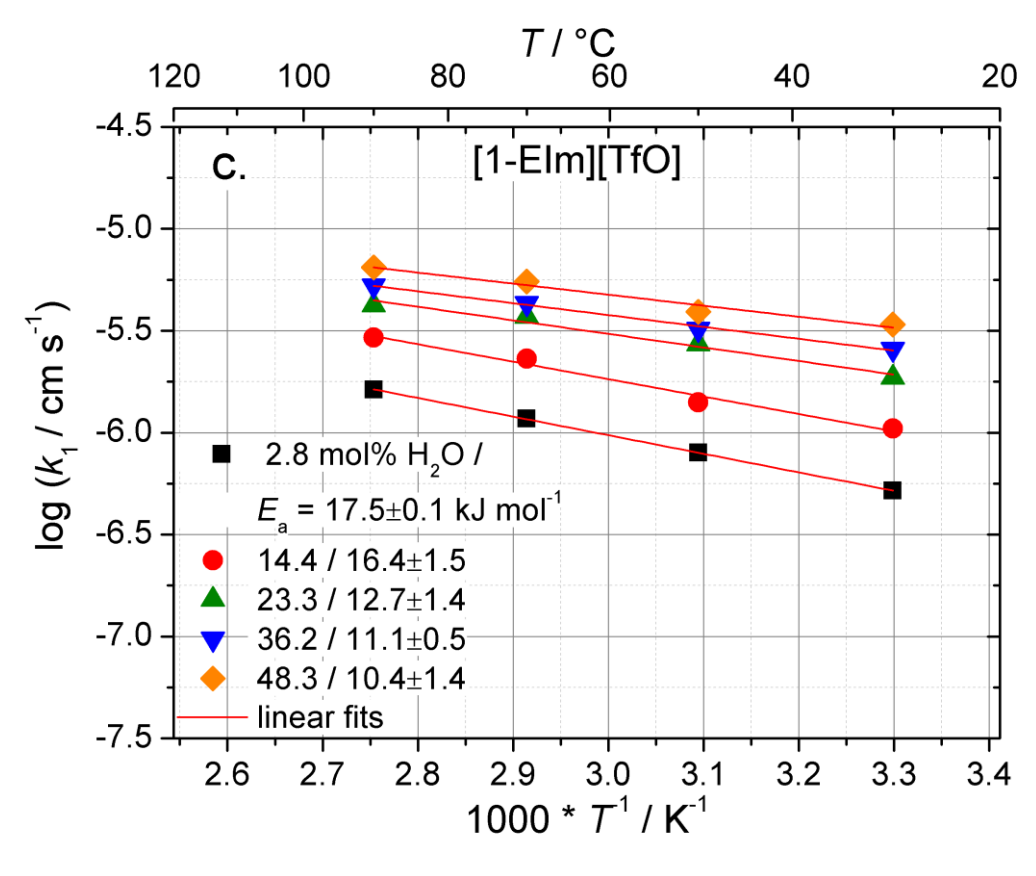


Figure 7







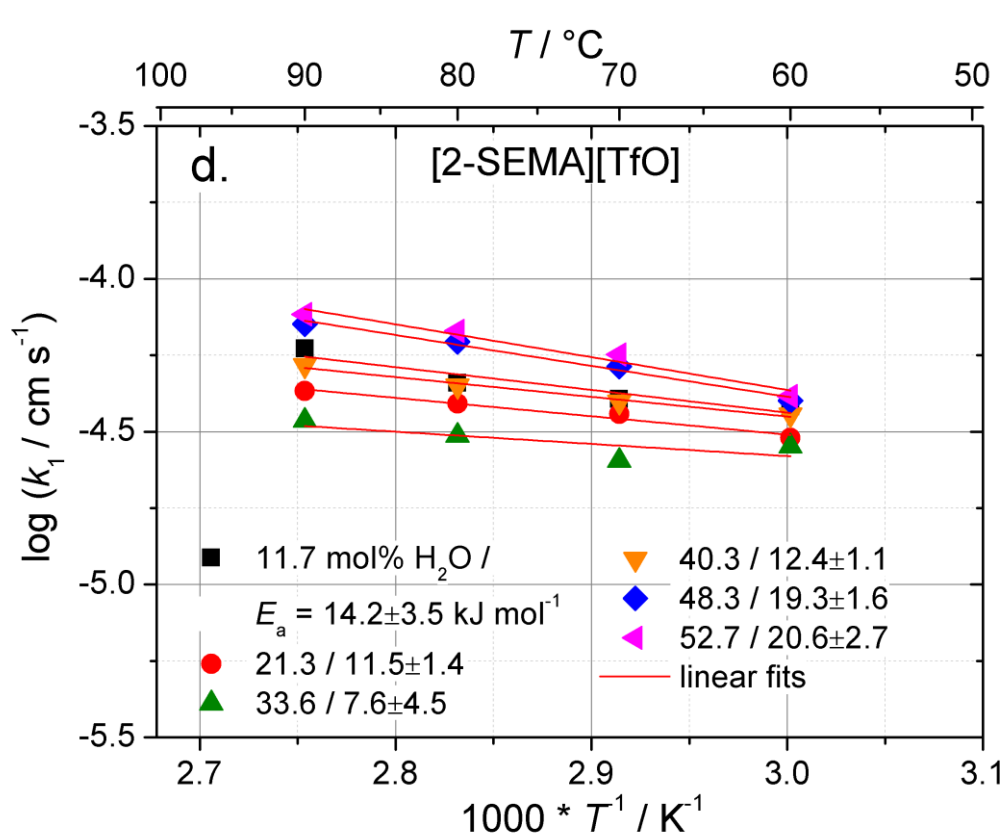


Figure 8

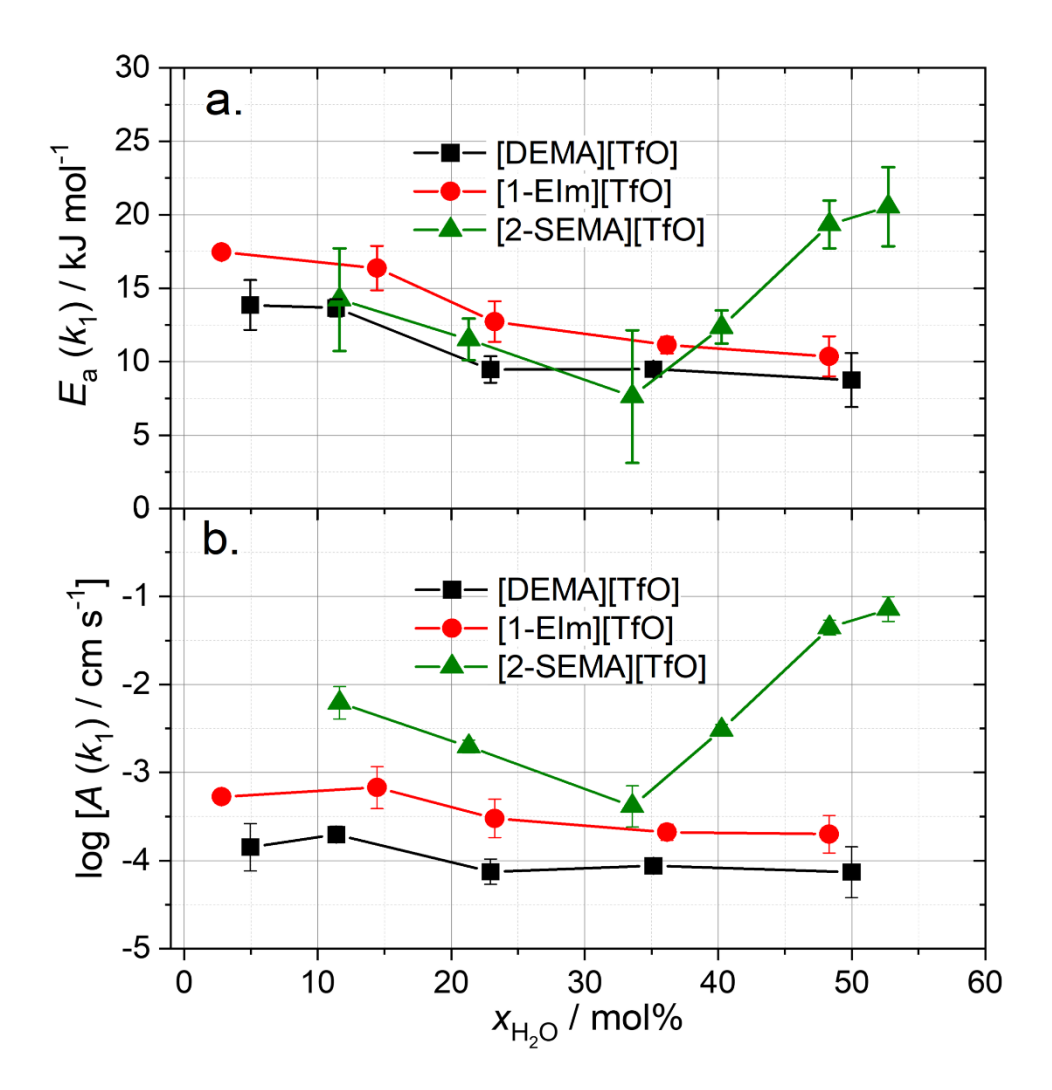


Figure 9

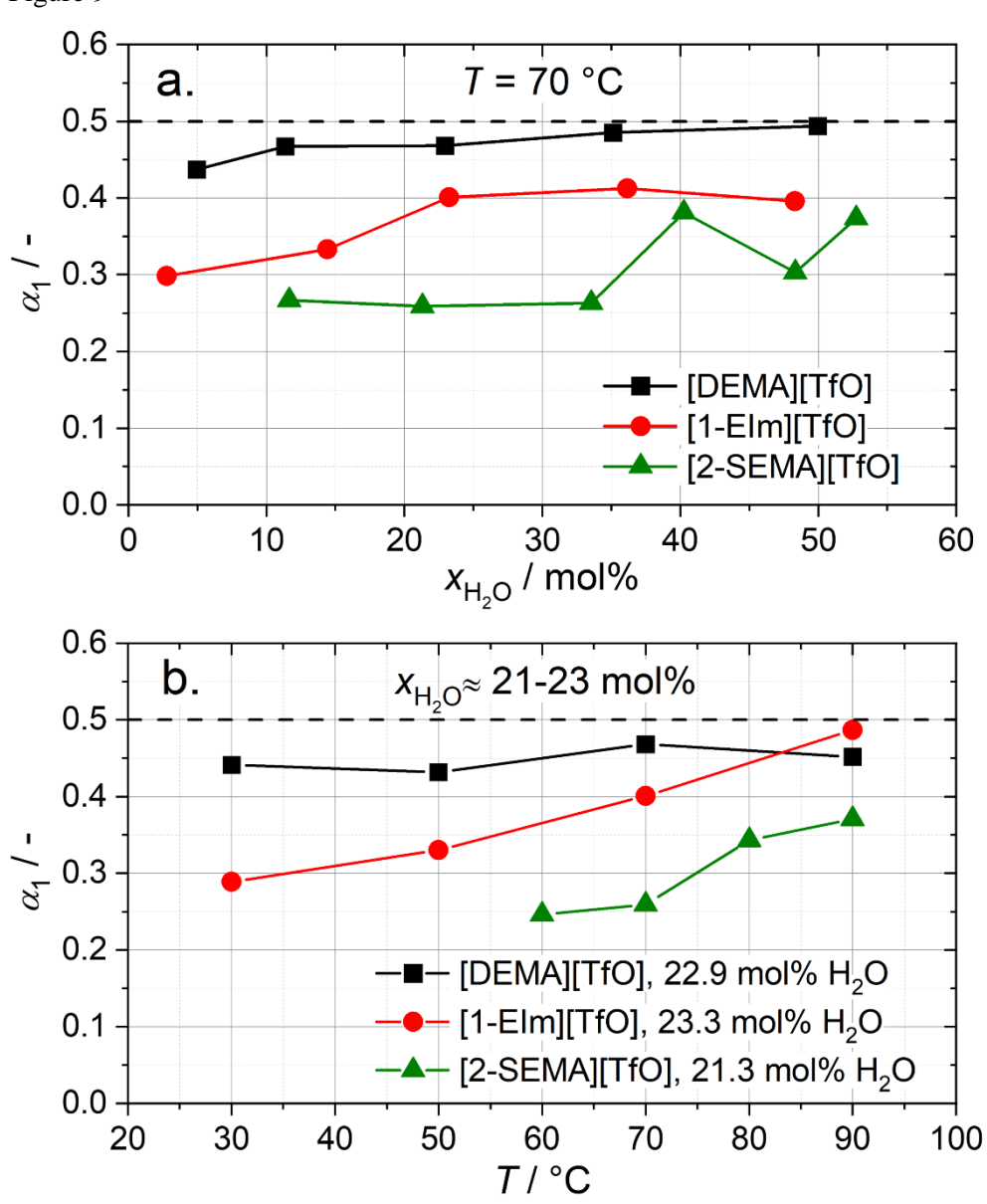


Table 1.

PIL	10 <sup>5</sup> D <sub>02</sub> / cm <sup>2</sup> s <sup>-1</sup>						
[DEMA][TfO]	x <sub>H2O</sub> / mol%	7/°C					
		30	50	70	90		
	5.0	0.39	0.47	0.55	0.63		
	11.4	0.43	0.53	0.64	0.74		
	22.9	0.50	0.64	0.78	0.92		
	35.1	0.57	0.76	0.94	1.12		
	50.0	0.68	0.92	1.17	1.41		
[1-Elm][TfO]	x <sub>H2O</sub> / mol%	T/°C					
		30	50	70	90		
	2.8	0.36	0.64	1.04	1.54		
	14.4	0.42	0.69	1.11	1.68		
	23.3	0.48	0.76	1.21	1.83		
	36.2	0.56	0.87	1.37	2.06		
	48.3	0.64	0.99	1.55	2.30		
[2-SEMA][TfO]	x <sub>H2O</sub> / mol%	T/°C					
		60	70	80	90		
	11.7	0.15	0.15	0.18	0.26		
	21.3	0.14	0.15	0.18	0.25		
	33.6	0.16	0.18	0.20	0.28		
	40.3	0.17	0.20	0.23	0.30		
	48.3	0.20	0.23	0.26	0.35		
	52.7	0.22	0.25	0.29	0.38		

Table 2.

PIL	10 <sup>6</sup> c <sub>02</sub> / mol cm <sup>-3</sup>						
[DEMA][TfO]	x <sub>H2O</sub> / mol%	T/°C					
		30	50	70	90		
	5.0	2.45	4.12	5.73	7.33		
	11.4	2.79	4.00	5.13	6.25		
	22.9	2.88	3.64	4.34	5.02		
	35.1	2.82	3.28	3.72	4.13		
	50.0	2.64	2.86	3.09	3.29		
[1-Elm][TfO]	x <sub>H2O</sub> / mol%	T/°C					
		30	50	70	90		
	2.8	2.40	2.34	2.28	2.23		
	14.4	2.70	2.52	2.34	2.14		
	23.3	2.65	2.45	2.23	2.01		
	36.2	2.52	2.30	2.07	1.83		
	48.3	2.38	2.15	1.92	1.68		
[2-SEMA][TfO]	<i>x</i> <sub>H2O</sub> / mol%	T/°C					
		60	70	80	90		
	11.7	0.63	0.85	1.03	1.24		
	21.3	0.73	0.90	1.06	1.23		
	33.6	0.80	0.93	1.07	1.20		
	40.3	0.84	0.94	1.07	1.19		
	48.3	0.87	0.95	1.06	1.16		
	52.7	0.88	0.95	1.06	1.15		